

CHEMICAL ABUNDANCES FOR EVOLVED STARS IN M5: LITHIUM THROUGH THORIUM⁸

DAVID K. LAI^{1,2}, GRAEME H. SMITH¹, MICHAEL BOLTE¹, JENNIFER A. JOHNSON³, SARA LUCATELLO^{4,5,6}, ROBERT P. KRAFT¹ AND CHRISTOPHER SNEDEN⁷

Draft version August 31, 2018

ABSTRACT

We present analysis of high-resolution spectra of a sample of stars in the globular cluster M5 (NGC 5904). The sample includes stars from the red giant branch (seven stars), the red horizontal branch (two stars), and the asymptotic giant branch (eight stars), with effective temperatures ranging from 4000 K to 6100 K. Spectra were obtained with the HIRES spectrometer on the Keck I telescope, with a wavelength coverage from 3700 Å to 7950 Å for the HB and AGB sample, and 5300 Å to 7600 Å for the majority of the RGB sample. We find offsets of some abundance ratios between the AGB and the RGB branches. However, these discrepancies appear to be due to analysis effects, and indicate that caution must be exerted when directly comparing abundance ratios between different evolutionary branches. We find the expected signatures of pollution from material enriched in the products of the hot hydrogen burning cycles such as the CNO, Ne–Na, and Mg–Al cycles, but no significant differences within these signatures among the three stellar evolutionary branches especially when considering the analysis offsets. We are also able to measure an assortment of neutron-capture element abundances, from Sr to Th, in the cluster. We find that the neutron-capture signature for all stars is the same, and shows a predominately r-process origin. However, we also see evidence of a small but consistent extra *s*-process signature that is not tied to the light-element variations, pointing to a pre-enrichment of this material in the protocluster gas.

1. INTRODUCTION

Among globular clusters of the northern sky, M5 is one of the nearest, and the element abundance patterns among its member stars have received considerable attention. On the basis of its observed proper motion, M5 actually appears to be an outer halo globular cluster on an eccentric orbit with a large apogalactic distance of ~ 60 kpc (Scholz et al. 1996). It is one of the most metal-rich globular clusters of the outer Galactic halo, with $[\text{Fe}/\text{H}] = -1.34 \pm 0.09$ (Carretta et al. 2009a).

M5 was one of the first globular clusters in which a sub-population of red giant branch (RGB) stars whose spectra exhibit enhanced $\lambda 4215$ CN bands were discovered via DDO photometry (Osborn 1971; Hesser et al. 1977; Pike 1978). The CN anomalies in M5 have been traced lower down the giant branch (Briley et al. 1992) and to the base of the RGB (Cohen et al. 2002). Abun-

dance variations of O, Na, and Al also exist among the RGB stars (e.g. Norris & Smith 1983; Ivans et al. 2001; Yong et al. 2008a,b; Carretta et al. 2009c,b), and inhomogeneities in Na abundance have been traced from the tip of the RGB to the main sequence turnoff by Ramírez & Cohen (2003). In all these respects, the abundance inhomogeneities found among RGB stars in M5 appear to be typical of the broad patterns found in other globular clusters of the Milky Way (e.g. Carretta et al. 2004; Gratton et al. 2001; Bragaglia et al. 2010) and also the Local Group (Mucciarelli et al. 2009).

However, abundance anomalies among the asymptotic giant branch (AGB) stars of globular clusters, including M5, have not been as well studied as those on the RGB. In color-magnitude diagrams (CMDs) of M5, the loci of the RGB and AGB are relatively clearly separated (see, for example, Simoda & Tanikawa 1970; Buonanno et al. 1981; Sandquist et al. 1996; Sandquist & Bolte 2004), making it a particularly useful cluster for studying AGB stars. Zinn (1977) classified a number of AGB stars as having very weak *G*-bands, and subsequently Smith & Norris (1993) found that a substantial fraction of AGB stars in M5 have enhanced CN band strengths. The presence of CN-strong stars on the AGB of various globular clusters has been reviewed by Sneden et al. (2000) and Campbell et al. (2006), based on the relatively sparse literature available. Table 1 in Campbell et al. (2006) suggests that in clusters more metal-poor than M5 the AGB stars tend to have weak CN bands. Campbell et al. (2010) confirmed a relatively large population of both CN-weak and CN-strong stars on the AGB of M5. This cluster therefore offers an opportunity for a more extensive study of N–Na–Mg–Al element enhancements on the AGB.

Two general mechanisms have been proposed to ex-

¹ UCO Lick/Department of Astronomy and Astrophysics, University of California, Santa Cruz, CA 95064; david@ucolick.org, bolte@ucolick.org, graeme@ucolick.org, kraft@ucolick.org

² NSF Astronomy and Astrophysics Postdoctoral Fellow

³ Department of Astronomy, Ohio State University, 140 W. 18th Ave., Columbus, OH 43210; jaj@astronomy.ohio-state.edu.

⁴ Osservatorio Astronomico di Padova, Vicolo dell'Osservatorio 5, 35122 Padua, Italy; sara.lucatello@oapd.inaf.it.

⁵ Excellence Cluster Universe, Technische Universität München, Boltzmannstr. 2, D-85748, Garching, Germany

⁶ Max-Planck-Institut für Astrophysik, Karl-Schwarzschild-Str. 1 85741 Garching, Germany

⁷ Department of Astronomy and McDonald Observatory, The University of Texas, Austin, TX 78712, chris@verdi.as.utexas.edu

⁸ The data presented herein were obtained at the W. M Keck Observatory, which is operated as a scientific partnership among the California Institute of Technology, the University of California and the National Aeronautics and Space Administration. The Observatory was made possible by the generous financial support of the W. M. Keck Foundation.

plain these abundance patterns (e.g., Kraft 1994). The first is that the surfaces of these stars are polluted during the RGB phase by the interior products of proton-capture reactions which have been consequently mixed to the surface. The second is that the stars with high N, Na, and Al and low O and C are part of a second generation of stars, formed out of gas ejected by polluters in which hot H burning took place. The nature of the polluters is still debated, including intermediate-mass AGB stars from $\sim 4\text{--}8 M_{\odot}$ (Ventura & D’Antona 2009), fast-rotating massive stars with $20\text{--}60 M_{\odot}$ (Decressin et al. 2007), and massive binaries with $\sim 20 M_{\odot}$ (de Mink et al. 2009). The discovery that these abundance patterns continue to at least the main-sequence turnoff indicates that these must be second-generation stars with the abundance anomalies throughout the entire star.

However, the surface abundances of some elements and isotopes are affected as stars go through the later phases of evolution (e.g., Gratton et al. 2000; Smith & Martell 2003). In addition to the first dredge-up on the low RGB, “deep mixing” or “extra mixing” on the upper reaches of the RGB causes C and Li abundance drops, N increases, and $^{12}\text{C}/^{13}\text{C}$ ratio decreases which were not predicted in original stellar models. This requires an additional physical effect that has not been conclusively identified. Possibilities include magnetic buoyancy (e.g. Busso et al. 2007; Denissenkov et al. 2009) and mean molecular weight gradients which lead to “thermohaline” mixing (Eggleton et al. 2006, 2008; Charbonnel & Zahn 2007). Part of the uncertainty lies in the efficiency of the mixing by either mechanism. For example, Charbonnel & Zahn (2007) showed that thermohaline mixing could account for the abundance patterns on the RGB if the efficiency for mixing was high, but two-dimensional simulations by Denissenkov (2010) of thermohaline mixing found that the actual efficiency was much smaller, closer to the magnitude in Kippenhahn et al. (1980).

There is also an ongoing debate about whether extra mixing happens on the AGB. Models without AGB extra mixing may have difficulty explaining observations of C/N and $^{12}\text{C}/^{13}\text{C}$ ratios in AGB stars (e.g., Lambert et al. 1986; Lebzelter et al. 2008; Milam et al. 2009) and O isotope ratios in pre-solar grains (e.g., Hoppe et al. 1997). Karakas et al. (2010) argued that if extra mixing on the RGB was included in the models, then no extra mixing on the AGB was needed to explain the C/N and C and O isotope ratios dredged up to the surface and observed in stars, at least at solar metallicities. Busso et al. (2010) found, however, that extra mixing in AGB stars was necessary to match isotope ratios in pre-solar grains, along with the C isotope ratios in C(N) stars, even if extra-mixing was included on the first ascent RGB. However, the mechanism for this extra mixing, like its counterpart on the RGB, is not yet known.

If deep mixing can also occur in AGB stars, then there is the possibility of CNO abundance differences being produced between the RGB and AGB. Recently, stellar models have been evolved from the main-sequence to the thermally pulsing AGB that includes mechanisms for mixing and extra mixing to trace the evolution of surface abundances in low-mass stars. Stancliffe (2010) focused on low-metallicity stars. Thermohaline efficiency was

adopted from Charbonnel & Zahn (2007) and is therefore very high. They found that ^3He is not all depleted, so thermohaline mixing could persist on the AGB. In addition, on the early AGB, the deepening of the convective envelope changes slightly the surface Li and ^3He abundances and the C isotope ratios.

In summary, theoretical work shows there are potentially interesting changes in the light elements resulting from mixing and extra mixing throughout the RGB and AGB. Observational evidence of the existence and size of these effects will constrain the mechanism of mixing and its efficiency. The AGB stars of M5 are cleanly separated from RGB stars, and the stars at the tip of the RGB provide a good reference for light-element abundances that may change on the AGB. In this paper we present measurements of light-element abundances for stars on both the RGB and AGB of M5 in an effort to determine whether there is any variation with stellar evolution.

The star-to-star inhomogeneities in the light elements of M5, however, do not appear to extend to the heavy elements formed by neutron-capture processes. This suggests that their production is divorced from the nucleosynthesis in the self-polluting cluster stars that made the second generation stars. The first in-depth study of Ba, La, and Eu in M5 from Ivans et al. (2001) found small internal scatter and good overall agreement with halo field subdwarfs with similar $[\text{Fe}/\text{H}]$. Interestingly, Ivans et al. (2001) noted that the abundances in M4 (Ivans et al. 1999) showed enhanced *s*-process contributions from AGB stars that enriched the natal gas of all stars in the cluster. Yong et al. (2008b) measured 27 elements heavier than Fe in two RGB stars in M5 and 12 RGB stars in M4. In addition to confirming the differences found by Ivans et al. (2001), they found that the abundance ratios could be explained by some *s*-process in M5 as well, though at a much smaller fraction than M4.

No freshly *s*-processed material is expected to appear on the surface of the present-day M5 AGB stars, because third dredge-up does not occur for stars with $M < 1.5M_{\odot}$. However, as is clear from the discussion of extra mixing, we do not fully understand the possible mixing events that can occur outside of the long-established dredge-up events, and the *s*-process elements for stars with a range of evolutionary states in M5 provide an opportunity to test models. For example, Masseron et al. (2006) suggest that the *s*-process enhancements seen in the extremely metal-poor AGB star CS 30322-023 are the result of an unknown mixing process that has brought this just-produced material to the surface. In this study, we also explore the origin of the neutron-capture elements in M5, and if there are any signatures of an *s*-process contribution.

2. OBSERVATION DETAILS

The stars observed for our investigation were chosen to sample the RGB, the RHB, and the AGB of M5. Much of our sample is covered by the photometric study of Sandquist & Bolte (2004), which shows a clear separation of the RGB from the AGB in their CMDs. The selection of targets was made so as to have a relatively broad coverage of each evolutionary branch up to the RGB tip luminosity, with a more uniform spread in the AGB to test for any subtle evolutionary effects that might occur.

Other than avoiding the most crowded central regions, no other selection was used in choosing targets. In Figure 1, we plot our sample within CMDs of M5 obtained from the *BVI* photometry of Sandquist & Bolte (2004).

The observation details along with photometry are presented in Table 1. All of the photometry data are taken from Sandquist & Bolte (2004), except for the RGB star I-65, which was taken from Buonanno et al. (1981). We have adopted a naming convention based on the compilation of Sandquist & Bolte (2004), where each star is designated by either A, R, or H based on whether it is an AGB, RGB, or HB star, respectively. The number following is based on the ordering in the respective photometry tables in Sandquist & Bolte (2004). However, one of the designated HB stars, HB13, seems to be better characterized as an AGB star (see Figure 1 and Tables 4 – 9). For added clarity, we add our own classifications to the last column of Table 1, along with designations from Arp (1955) where available.

Our spectra were obtained using the HIRES spectrograph on the Keck 1 telescope (Vogt et al. 1994). On 2007 June 5–7 we observed the AGB, HB, and part of our RGB sample with the recently upgraded detector focal plane, a setup that provided near continuous wavelength coverage between 3700 and 7950 Å. The remainder of the RGB sample is from an earlier run on 2000 June 6 with the original HIRES CCD, and therefore covers a more limited wavelength range of 5300–7600 Å.

3. STELLAR PARAMETERS AND ANALYSIS

3.1. Reductions and Model Atmospheres

We reduced our spectra using the MAKEE data reduction package⁹. Equivalent widths (EWs) were measured using the SPECTRE program (Fitzpatrick & Sneden 1987) by fitting Gaussian profiles. For strong lines with extended wings, direct integration of the line profile was used to measure the EW.

The line list was based partially on those used in Ivans et al. (2003) and Ramírez & Cohen (2003) and, when available, the *gf* values were updated with more recent measurements. Many additional lines, predominantly in the blue region, were also included. We present EWs and atomic parameters with *gf* references in Table 2. In Figure 2 the measured EWs are compared with those of Ivans et al. (2003) and Ramírez & Cohen (2003) respectively. There is one star overlapping with both studies, A11 (IV-59). In both cases we have on average slightly smaller EWs, the consequences of which are discussed in Section 4.1.

We adopted the model atmospheres computed by Kirby et al. (2009). These were built on the ATLAS9 model atmospheres (Kurucz 1993), using updated opacity distribution functions (Castelli 2005). In this grid of atmospheres we set to $[\alpha/\text{Fe}] = 0.3$ in all cases based on previous studies (Ivans et al. 2001; Ramírez & Cohen 2003). In practice, the final abundance results are fairly insensitive to variations in the adopted $[\alpha/\text{Fe}]$ ratio of the model atmosphere. We then interpolated the atmospheres to the final T_{eff} , $\log g$, and $[\text{Fe}/\text{H}]$ values. The derivation of the parameters is described in Section 3.2. The current version of the local thermodynamic equi-

librium (LTE) spectral analysis code MOOG¹⁰ (Sneden 1973) was then used for the EW and spectral synthesis abundance determinations.

We accounted for hyperfine splitting (HFS) in the Sc II, V I, Mn I, Co I, and Cu I lines with the HFS parameters given by Kurucz¹¹. We used the HFS parameters from McWilliam (1998), Lawler et al. (2001b) and Lawler et al. (2001a) for the Ba II, Eu II and La II abundance determinations, respectively. The Th II abundance was determined from spectral synthesis of the 5989 Å transition with the *gf* value from Nilsson et al. (2002). Using the line parameters from Lucatello et al. (2003), the C abundance and χ values were determined from spectral synthesis of the CH *G*-band regions near 4234 and 4360 Å, and N was determined from the CN band at 3880 Å.

3.2. Stellar Parameters

We took a hybrid approach for deriving the stellar parameters. The T_{eff} value for each star was spectroscopically set by eliminating any abundance trend determined from individual Fe I lines with their excitation potential (excluding lines with excitation potential ~ 0.0 eV). This, in practice, gives very good agreement to the T_{eff} calculated with the $B - V$ and $V - K$ color- T_{eff} relationship from Ramírez & Meléndez (2005), with K magnitudes from the Two Micron All Sky Survey (2MASS, Skrutskie et al. 2006), and reddening of $E(B - V) = 0.03$ (Harris 1996). The microturbulent velocity (v_t) was set in the usual manner by eliminating any trend of individual Fe I line abundances with EW.

For the $\log g$ determination we chose to use the known distance to M5 instead of ionization balance. This requires using additional information, specifically the distance modulus, the stellar mass, and the bolometric correction (BC) for each star. We adopt the distance modulus given by Kraft & Ivans (2003), and following Ivans et al. (2001), assume a mass of $0.80 M_{\odot}$ for the RGB sample and $0.70 M_{\odot}$ for our AGB and HB sample to account for expected mass loss. This value may be slightly high, at least when comparing to mass estimates from RRc Lyrae in M5. Clement & Shelton (1997) and Kaluzny et al. (2000) calculate average masses for their samples of RRc Lyrae stars at 0.58 and $0.54 M_{\odot}$, respectively. However, assuming a mass of $0.60 M_{\odot}$ generally decreases the $\log g$ by approximately only 0.07 dex, and therefore has little affect on the abundance determinations. Given the small change to $\log g$, we use the $0.70 M_{\odot}$ value for consistency with Ivans et al. (2001). We then use the BCs from Houdashelt et al. (2000). Similar to the technique described in Ramírez & Cohen (2003), the tables of Houdashelt et al. (2000) are interpolated over $[\text{Fe}/\text{H}]$, T_{eff} , with a first guess value of $\log g$ to get an initial value of BC. This was then used to recalculate $\log g$. The procedure was iterated until self-consistent values were obtained for both BC and $\log g$.

Our method of deriving $\log g$ using the known distance to M5 gives different values than the traditional spectroscopic ionization balance technique (Figure 3). This is discussed in great detail for M5 in Ivans et al. (2001),

⁹ <http://spider.ipac.caltech.edu/staff/tab/makee/>

¹⁰ <http://verdi.as.utexas.edu/moog.html>

¹¹ <http://kurucz.harvard.edu/linelists.html>

and more generally for clusters in Kraft & Ivans (2003). In short, the possibility of unaccounted for effects, e.g., non-LTE (NLTE) effects, will most greatly affect the neutral Fe I species (Thévenin & Idiart 1999). Therefore the final adopted $[\text{Fe}/\text{H}]$ for our model atmospheres is chosen to agree with the final derived $[\text{Fe II}/\text{H}]$ value within 0.1 dex, instead of the $[\text{Fe I}/\text{H}]$ value. Our final atmospheric parameters are given in Table 3. The radial velocities of each star are also presented in Table 3, with the error on each measurement approximately 1 km s^{-1} (Griest et al. 2010).

Another important feature shown in Figure 3 is the offset between the Fe abundances derived for each evolutionary state. The AGB stars show consistently lower Fe I and Fe II abundances compared to the RGB stars. The RGB abundances are on average 0.16 dex higher in Fe I than for the AGB part of the sample. This is almost the same as the 0.15 dex offset found by Ivans et al. (2001). We also find a similar offset in the Fe II values of 0.13 dex in the same direction (here Ivans et al. 2001 find only a 0.06 dex difference). The two HB stars also show a large difference in their Fe I–Fe II values, along with an offset from the AGB and RGB stars.

We take the suggestion of our referee, and explore if the variations in the number of Fe II lines used in each star has an effect on the offsets among the different evolutionary branches. First we define a subset of Fe II lines that are generally present in the stars of the whole sample. This comes out to six lines, of which there is an average of ~ 5 measured per star. Interestingly, the AGB sample then gives on average a $+0.04$ dex offset in $[\text{Fe II}/\text{H}]$ when using only these lines, while the HB sample is offset by $+0.02$ dex, and the RGB has no change on average. The difference in the line list could account for some of the offset, but there remains an unexplained significant difference in the values of $[\text{Fe II}/\text{H}]$. These differences seem to point to problems in our standard one-dimensional, LTE analysis when dealing with these evolved stars. The caution most strongly applies to absolute abundances, and is minimized somewhat by considering abundance ratios. This is discussed further in Section 5.1.

3.3. Calculation of Abundance Errors

We follow the abundance-error analysis technique described in Johnson (2002), which includes the dependences among T_{eff} , $\log g$, and v_t . To estimate the component of the error arising from EW measurements and uncertainties in atomic parameters, we used the standard error based on the standard deviation of the abundances derived from multiple lines. For abundances with four or fewer individual line measurements, we assumed a conservative 0.15 dex lower limit for the standard deviation.

For the atmospheric parameters, we assume errors of 100 K in T_{eff} , 0.2 dex in $\log g$, and 0.2 km s^{-1} in v_t . The T_{eff} and v_t errors are motivated by the sensitivity of the Fe I line abundances. Changes of the order of 100 K and 0.2 km s^{-1} and larger in T_{eff} and v_t , begin to introduce large trends of Fe I with excitation potential and EW, respectively. For the $\log g$ error, we follow the calculations of Ramírez & Cohen (2003), which combine uncertainty in distance, stellar mass, and T_{eff} , to arrive at the value of 0.2 dex.

We then calculated the abundance errors due to atmospheric uncertainties using three representative stars, a

low- T_{eff} star (to be used for stars with $T_{\text{eff}} < 4500 \text{ K}$), a moderate- T_{eff} star (for the temperature range $4500 \leq T_{\text{eff}} < 5000 \text{ K}$), and a high- T_{eff} star (for $T_{\text{eff}} \geq 5000 \text{ K}$, which applies only to the two hottest HB stars). These errors were then applied to each star in the T_{eff} ranges noted above. The final combined errors are then calculated using Equations (5) and (6) in Johnson (2002).

4. RESULTS

Our abundance results are summarized in Tables 4–9. In Table 10 we give the average values, the standard deviation σ , and number of measurements for each abundance ratio for both the entire sample and for each evolutionary branch. We take the solar photospheric abundances from Anders & Grevesse (1989), but for Fe we use solar $\log \epsilon(\text{Fe}) = 7.52$. We note that for recent compilations of the solar abundances (e.g., Asplund et al. 2009; Lodders et al. 2009) a three-dimensional analysis gives C, N, and O abundances appreciably different from Anders & Grevesse (1989). However, because we are performing a one-dimensional analysis, we use the Anders & Grevesse (1989) results. The neutral species ratios are reported relative to Fe I and the ionized species ratios are reported relative to Fe II. All abundances reported without an ionization state are neutral, and are explicitly labeled as such when both neutral and ionized states are measured for a given element.

The one exception to this is $[\text{O}/\text{Fe}]$. With their high excitation potentials, the abundance determined from the O triplet lines at 7770 \AA are taken relative to the Fe II abundance. The value determined from the forbidden O lines at 6300 and 6363 \AA are still expressed relative to Fe I. When lines from both sets of transitions are measured, these relative values are combined to obtain the final $[\text{O}/\text{Fe}]$ given in Table 4. Shown in Figure 4 are the $[\text{O}/\text{Fe}]$ abundances derived from the triplet lines and the forbidden lines in the six stars where both sets of lines are measured. In these cases, we find good agreement between both abundance ratio determinations when using this method.

We also apply NLTE corrections for abundances determined from the O triplet lines and the Na lines. These corrections were applied line by line by extrapolating the tables from Gratton et al. (1999) between EW, metallicity, T_{eff} , and $\log g$. It is important to note that the NLTE corrections for Na from Gratton et al. (1999) can be in the opposite direction from other studies (see the review by Asplund (2005)). However, we adopt the Gratton et al. (1999) study because of the ability to extrapolate the NLTE corrections over a wide range of EW, T_{eff} , and $\log g$ values, which is vital to this study. Since we consistently use the Gratton et al. (1999) corrections, this should leave the relative abundance trends in this study intact. However, this may lead to systematic differences with other studies that use different sets of NLTE corrections for Na (e.g., Baumüller et al. 1998; Mashonkina et al. 2000; Shi et al. 2004).

4.1. Comparison to Previous Studies

We compare our atmospheric parameters and abundance measurements for the star A11 to those determined by Ivans et al. (2001) and Ramírez & Cohen (2003) in Table 11. The results of Ramírez & Cohen (2003) are converted to be relative to the Anders & Grevesse (1989)

solar values to be consistent with our abundance ratios. The atmospheric values in the different studies are in good agreement. We find lower [Fe I/H] and [Fe II/H] values, which can at least be partially explained by our slightly smaller EW values. However, when we compare abundance ratios we find generally good agreement with these previous studies. The exceptions to this seem to be [Si/Fe], [Sc II/Fe], and [Cu/Fe].

To test the effects of the EW offsets we ran two sets of abundance determinations with our measured EWs increased by 7.92 and 2.62 mÅ, to match the offsets found between our study and Ivans et al. (2001) and Ramírez & Cohen (2003), respectively. In both cases all abundance ratios relative to Fe remained virtually unchanged. However, the [Fe I/H] and [Fe II/H] abundances did experience shifts. For the Ivans et al. (2001) EW shift we calculate [Fe I/H] = -1.37 and [Fe II/H] = -1.27 , in excellent agreement with their values of -1.40 and -1.25 . For the Ramírez & Cohen (2003) EW shift we calculate [Fe I/H] = -1.51 and [Fe II/H] = -1.41 , which within the errors is in agreement with their values of -1.40 and -1.35 .

The discrepancies still remain for [Si/Fe], [Sc II/Fe], and [Cu/Fe]. The differences in abundance ratios are unlikely to be due to atmospheric parameters given the good agreement between those adopted in the various studies and the insensitivity of abundance ratios to the correspondingly small differences (see, for example, Table 3 in Ivans et al. 2001).

One possibility lies in the different sets of lines and/or log gf values adopted here versus the previous studies. We test this by deriving abundances based only on lines that overlap with Ramírez & Cohen (2003) along with their log gf values. We do not perform this same exercise with Ivans et al. (2001) because there are only 32 overlapping lines (versus 236 lines from Ramírez & Cohen 2003), making the comparison less useful. The only significant deviation comes in the [Cr I/Fe] abundance ratio, which we find to be 0.24 dex higher when using only overlapping lines. This is not due to log gf values, as we have adopted the same values from Ramírez & Cohen (2003). The difference comes in the small number of overlap lines in Cr I, only three in this case as compared to the 24 lines we use in the final analysis of this star. These three lines give a relatively large scatter using either set of EWs. With the exception of [Cr I/Fe], however, the abundance results that can be measured with this overlapping subset of lines remain the same within errors.

To test the effect of using different atmosphere models, we ran an abundance analysis on our A11 data using a MARCS model atmosphere with an alpha enhancement of 0.4 (Gustafsson et al. 2008). The results of this exercise are also presented in Table 11. The only atmospheric parameter that needed an adjustment was v_t . Overall there is little change between the abundances derived from our adopted atmosphere or the MARCS model atmosphere, with any of the differences well within the errors. The lower [Fe I/H] and [Fe II/H] values remain, and the [Si/Fe], [Sc II/Fe], and [Cu/Fe] values also remain very similar. Thus the sources of the differences in these three particular [X/Fe] ratios between the present work and the studies of Ivans et al. (2001) and Ramírez & Cohen (2003) remain unidentified.

5. DISCUSSION

5.1. Abundance Comparisons

If there are no systematic errors in our analysis and if no changes in the surface abundances with evolutionary phase, then we should see the same patterns when we compare the RGB, HB and AGBs and when we compare our results with the literature values. However, there are several cautionary points that need to be made before such comparisons are attempted.

5.1.1. Absolute Abundances

As can be seen in Figure 3, there are some difficulties in interpreting certain absolute abundances from our analysis. Most notably, the Fe abundance appears to change with evolutionary state. Korn et al. (2007) find that atomic diffusion could operate on unevolved stars near the turnoff and hence modify the surface abundance of elements such as iron. However, when looking at stars evolved past the lower RGB, this mechanism only seems to affect hotter BHB stars ($T_{\text{eff}} > 8500\text{K}$, e.g., Behr et al. 2000). For our sample of cooler and evolved stars no internal processes are known to modify the surface iron abundance of globular cluster stars, which leads us to suggest that the trend in Figure 3 is artificial. Thus, comparisons between the absolute abundances of other elements between the RGB, AGB, and HB stars may also contain unaccounted for systematic effects.

There are some ways to minimize this problem. One method, when available, is to compare abundance values that are less prone to effects that potentially have significant repercussions on the analysis, such as three-dimensional atmosphere and NLTE effects (e.g., Asplund 2005; Asplund et al. 2009). For example, in Figure 3, [Fe II/H] shows a far more consistent value than [Fe I/H]. This is probably because in the stellar conditions of the stars we are analyzing [Fe II/H] is the majority species, and therefore less prone to showing NLTE effects that we cannot account for. Another approach to the problem is to use pre-determined corrections for NLTE, as we have done for O and Na.

These concerns raise the issue of how to best compare the metallicity derived here for M5 to results of previous studies. Given that the majority of stars in prior studies are not evolved past the RGB phase, the most meaningful comparison may be to only consider RGB stars in our sample (note, though, that the direct star-to-star comparison discussed in Section 4.1 is for an AGB star). We also recommend only comparing [Fe II/H] abundances instead of [Fe I/H] for the reasons given above. As reported in Table 10, we find for our RGB sample an average [Fe II/H] = -1.33 . This compares well to recent high-resolution studies giving [Fe II/H] values of -1.27 (Koch & McWilliam 2010), -1.32 (Carretta et al. 2009b), -1.33 (Ramírez & Cohen 2003), and -1.20 (Ivans et al. 2001). All of these values have been scaled to our adopted solar abundance of $\log \epsilon(\text{Fe}) = 7.52$, and only include stars that have not evolved past the RGB.

5.1.2. Abundance ratios

To minimize the effects of absolute abundance offsets, we now limit our discussion to comparisons of abundance ratios, and discuss element abundances relative to either

Fe I or Fe II. This assumes that the same NLTE, three-dimensional, and other issues affect the abundance determinations of individual elements in a similar manner. However, this still leaves some uncertainty, as illustrated in Figures 5, 6, and 7. For the abundance ratio of $[\text{Ca}/\text{Fe}]$ shown in Figure 5, we find an offset depending on a star's evolutionary state. An offset is even more apparent for $[\text{V}/\text{Fe}]$, shown in Figure 6. In the case of $[\text{Mg}/\text{Fe}]$, an abundance ratio that has been shown to vary in globular clusters, Figure 7 shows that our values are consistent within the errors with a constant value across all observed stars (and also consistent with Carretta et al. 2009b who found no Mg variation in a sample of 14 M5 RGB stars).

The abundances of Ca and V, like Fe, can only be modified by previous stellar generations via supernovae ejecta, and therefore should not vary as a star evolves. While Mg can be modified by the Mg–Al cycle, the direct evidence of this is generally difficult to detect given the large absolute amount of Mg in a star relative to the absolute amount of Al present. This makes any potential systematic errors in the $[\text{Mg}/\text{Fe}]$ ratio easily able to mask true signs of variation. For $[\text{Ca}/\text{Fe}]$ and $[\text{V}/\text{Fe}]$, which we expect should be constant, it seems that there are systematic errors that give the appearance of abundance differences between AGB and RGB stars. The offset is 0.15 dex in the case of $[\text{V}/\text{Fe}]$. This is the largest abundance offset between the AGB and RGB for elements heavier than Al and with greater than one measurement on each branch (see Table 10). We can take this as a conservative lower limit to our true abundance ratio uncertainty when comparing stars from different evolutionary states. A possible method to reduce these effects is to use the differential analysis as described in Koch & McWilliam (2008, 2010). However the wide range of effective temperatures in our sample would both make this type of analysis impractical and still make star-to-star comparisons problematic.

The potential for such systematic effects has ramifications beyond comparing the different stellar evolution branches of M5. A recent example comes from efforts to ascertain whether Ca varies within globular clusters, and the implications for the origin of light element variations found in these systems (Lee et al. 2009). Carretta et al. (2010a) find from their large sample of globular cluster red giant stars that Ca does not vary significantly in a given cluster. M5 has a fairly cleanly separated AGB, unlike some other globular clusters. Therefore, even though Carretta et al. (2009a) show that AGB star contamination is low in their sample, any AGB contamination could artificially inflate star-to-star Ca variations. This effect would tend in the direction of making their findings of already low Ca variations an upper limit.

5.2. Abundance Inhomogeneities among the Lighter Elements Li through Mg

Given the caveats above, we do find true abundance variations in the lighter elements of C through Al among the stars in our M5 sample. Interesting changes in C, N, Li and the C isotopes may potentially occur between the tip of the RGB and the onset of the thermally pulsing AGB depending on (1) the existence and strength of extra mixing and (2) the depth from which any of the material with O–Na–Al abundance anomalies orig-

inates. Detecting these changes in M5 is complicated by the dispersion in these abundances for stars in all evolutionary states. In the following sections, we explore if there is evidence for any additional mixing or changes on the AGB branch that manifest themselves in surface abundances, and how our sample fits into the context of previous studies of M5.

5.2.1. C, N, O and $^{12}\text{C}/^{13}\text{C}$ among the Different Branches

The light elements C, N, and O show variations that do not seem to be correlated with either evolution along a particular evolutionary branch (for which surface gravity is a proxy) or among different evolutionary branches as a whole (Figure 8). Thus we do not see any evidence for additional mixing within AGB stars compared to the upper RGB stars in our sample. The HB stars have the highest measured $[\text{O}/\text{Fe}]$ abundances, but given the differences in effective temperature, and to a lesser extent surface gravity, between the HB stars and those of the RGB and AGB, a claim of a truly intrinsic $[\text{O}/\text{Fe}]$ enhancement in the HB stars is not made here.

Perhaps a more definitive test for evolutionary differences between AGB and RGB stars is provided by the measurement of the $^{12}\text{C}/^{13}\text{C}$ ratio, which is less sensitive to model atmosphere uncertainties. This ratio can be altered by the CNO cycle of H-burning reactions. In Figure 8 the $^{12}\text{C}/^{13}\text{C}$ ratio is also plotted versus surface gravity for the AGB stars and the two RGB stars for which it could be measured. The values are all consistent within the errors to be around 5.5, close to the CNO cycle equilibrium value of 3.5. There is no difference between the RGB and the AGB stars, and no change with AGB evolution. In particular, the low C isotope ratios measured here are consistent with values found for three red giants in M5 by Pavlenko et al. (2003), as well as with values found on the upper RGBs of other globular clusters and in halo field red giants (e.g., Brown & Wallerstein 1989; Gratton et al. 2000; Keller et al. 2001; Pavlenko et al. 2003; Shetrone 2003; Recio-Blanco & de Laverny 2007).

In the context of the AGB models of Stancliffe (2010), we do not see any drop in the $^{12}\text{C}/^{13}\text{C}$ going up the AGB as might be expected from the thermohaline mixing assumed in their models. However, AGB stars in M5 are at a higher metallicity and are slightly lower mass than the most appropriate model of Stancliffe (2010), so an exact comparison cannot be done. Also, it appears that the AGB stars of M5 start with a much lower $^{12}\text{C}/^{13}\text{C}$ ratio than their models, which could make surface modifications to this ratio difficult to detect.

5.2.2. Evidence of the CNO cycle

With only two RGB stars with $[\text{C}/\text{Fe}]$ and $[\text{N}/\text{Fe}]$ measurements, along with possible systematic differences in atmospheres between RGB and AGB stars, we generally limit the comparison of the CNO behavior within the sample of AGB stars. The C–O correlation and C–N anticorrelation expected from varying degrees of CNO cycling of material appear to be present (Figure 9). The scatter in the N versus O plot is large enough to preclude any conclusions as to the presence of an N–O anticorrelation.

We also see constant C+N+O in our sample, consistent with the material in these stars having undergone

CNO cycling in the first generation of stars, in early RGB phases, or both. In Figure 10, we show that the combined $[C+N+O/Fe]$ ratio depends on neither evolution nor other light-element variations. Combined with the lack of correlation of C, N, O, and $^{12}C/^{13}C$ with evolutionary state, this is an indication that while the CNO cycling of material occurred, we do not find evidence for extra mixing having occurred between the RGB tip and the TP–AGB phase of M5 in any appreciable manner.

These results for the AGB are analogous to those found on the subgiant branch by Cohen et al. (2002) and the RGB by Sneden et al. (1992) and Ivans et al. (2001). The presence of N-enhanced stars extending from the subgiant branch to the AGB implies that they contain material that has been processed through the CNO cycle of hydrogen burning prior to their formation.

5.2.3. $[C/Fe]$ and $[N/Fe]$ as Compared to Previous Studies

The wavelength coverage for the majority of the RGB sample precluded measurement of $[C/Fe]$; however, we find the average $[C/Fe]$ of the two RGB stars we could measure, R9 and R21, is found to be -0.25 dex. Previous studies of $[C/Fe]$ in M5 have found values on the order of 0.2 – 0.4 dex lower, albeit using different techniques (Langer et al. 1985 and Smith et al. 1997 from low-resolution spectroscopy of the G band, and by Pavlenko et al. 2003 from the $2.3 \mu\text{m}$ CO bands).

We can further compare our entire sample of $[C/Fe]$ and $[N/Fe]$ measurements to previous studies of M5. In particular, we use the work of Cohen et al. (2002), because of their large sample size. In Figure 11, we compare the distributions of $[C/Fe]$, $[N/Fe]$, and $[C/N]$. Our sample is more $[C/Fe]$ -enhanced and slightly $[N/Fe]$ deficient relative to that of Cohen et al. (2002). This translates to an enhancement of $[C/N]$ in our sample. If anything, because the stars from Cohen et al. (2002) fall below the RGB bump, one would expect from deep mixing that our sample would have lower $[C/Fe]$ and higher $[N/Fe]$ distributions.

One possible explanation for these discrepancies is systematic offsets of CNO abundance ratios between the two giant branches as discussed in Section 5.1.1. However, except for $[N/Fe]$, the RGB sample shows similar distribution of values in $[C/Fe]$ and $[O/Fe]$ as the AGB sample. Another possible explanation is a systematic difference between our high-resolution abundance analysis and previous work using CH and CN indices such as done in Cohen et al. (2002).

Although systematic errors cannot be ruled out, one intriguing possibility is that this discrepancy is related to the finding of Campbell et al. (2010) that there is a relatively large number of CN-weak stars on the AGB of M5 relative to the CN-weak stars on the RGB. Given that Cohen et al. (2002) is a study of subgiant stars, and our sample is predominately AGB stars, our higher peaked $[C/N]$ distribution would be expected from the Campbell et al. (2010) result. Physically, this may be related to high-N stars on the RGB having increased mass-loss rates. This leads these stars to evolve to the bluer end of the HB, and possibly never making it to the AGB (Norris et al. 1981; Campbell et al. 2010).

5.2.4. Li

We are only able to measure Li in three of our stars, using spectral synthesis of the $\lambda 6708$ Li resonance doublet. In the red giants R394, I-65, and R431, which sit right at the RGB bump at $V = 14.99$, we find $\log\epsilon(Li) = 0.76, 0.73, \text{ and } 0.96$. For all other stars in our sample, Li could not be detected and we find upper limits of $\log\epsilon(Li) < 0$. These $\log\epsilon(Li)$ values are intermediate to the values found by Gratton et al. (2000) for field RGB stars of similar metallicities below the RGB bump ($\log\epsilon(Li) \simeq 1.15$) and above it ($\log\epsilon(Li) < 0$). They are also consistent with the $\log\epsilon(Li)$ values found on the RGB bump of M4 found by D’Orazi & Marino (2010).

These measurements support the notion that deep mixing is performing as expected from these previous studies on the RGB of M5. Unfortunately, because we have only three stars at the RGB bump, we cannot comment on the potential difference in the evolution of $\log\epsilon(Li)$ value for Na-rich and Na-poor stars as D’Orazi & Marino (2010) find in M4. However, our consistent finding with the field and M4 suggests M5 as being a promising cluster for a similar study.

5.2.5. $Na, Al, \text{ and } Mg$

The C, N, O, and Na abundances show the expected (anti)correlations if the CNO cycle took place in the same location as the Ne–Na cycle (Figure 12). In the same figure we also show the C, N, and O abundances as a function of $[Al/Fe]$. Similar correlations as with $[Na/Fe]$ are indicative of the Mg–Al cycle, which we discuss more below. In Figure 13, both $[Na/Fe]$ and $[Al/Fe]$ show no trends with evolution, as would be expected in the self-pollution scenario.

An Mg–Al anticorrelation, however, arising from the Mg–Al cycle is uncertain. In Figure 14, the variation in Mg is primarily driven by two points and within errors is consistent with having no anticorrelation, agreeing with the findings of Carretta et al. (2009b). Given the discussion in Section 5.1.1, this is hardly surprising. However, a strong correlation in Na–Al is clearly present in Figure 14. Taken with the behavior of the CNO abundances with $[Al/Fe]$ shown in Figure 12, this strongly suggests the presence of the Mg–Al cycle.

In Figure 15 we show how our Na–Al correlation compares to the previous M5 studies of RGB and AGB stars in Ivans et al. (2001) and RGB stars in Carretta et al. (2009c). The offset between the correlation found from our data (plotted as a solid line in 15) and the Ivans et al. (2001) values is almost exactly accounted for by different gf values adopted in our Al abundance determinations. We updated the Al gf values used by Ivans et al. (2001) for the $\lambda 6696$ and $\lambda 6699$ transitions to current values given by NIST, which are very similar to the gf values used in Carretta et al. (2009c). With the offset accounted for, the trend we find matches both of the previous studies very well.

Given the correlations described above, it is likely that the CNO, Ne–Na, and Mg–Al cycles operated in a common site that has influenced the abundances of some fraction of M5 stars. Our data cannot discern between self-pollution of the observed M5 stars via deep mixing, or a primordial scenario giving rise to these observational signatures. However, the studies of unevolved stars in M5 by Cohen et al. (2002) and Ramírez & Cohen (2003) find that these relationships exist in earlier stellar evolution-

ary branches in M5. With our match to previous work on the Na-Al correlation, we are consistent with the picture of multiple generations of stars giving rise to heterogeneous self-enrichment of the light elements in globular clusters, a scenario that was introduced in an early form by Cottrell & Da Costa (1981), and which has been discussed and expanded upon in a number of papers, such as the recent work by Carretta et al. (2010b).

5.3. The Neutron-capture Signature

We are able to measure many neutron-capture transitions in our spectra. This provides an opportunity to better understand the nucleosynthetic footprint of the neutron-capture processes that have occurred in the stars of M5. Coupled with the sample selection of AGB stars, we can also check for any early onset of *s*-process dredge-up.

In Figure 16, we plot all of our measured neutron-capture element abundances and compare them to the scaled solar system *r*-process pattern. The abundances match the scaled solar system *r*-process pattern fairly well, and there is also a very small star-to-star scatter in each abundance. For example, if we take [Eu/Fe], an element almost entirely synthesized in the *r*-process, we find an average value of [Eu/Fe]= 0.44 ± 0.02 ($\sigma = 0.09$). This average value agrees very well with the larger sample of Ivans et al. (2001), but we find an even smaller scatter than that study. The lack of star-to-star scatter also falls in line with most other globular clusters, unlike in the case of M15 (Snedden et al. 1997).

To attempt to take out the effect of even this small star-to-star scatter, we compare our neutron-capture abundances relative to Eu in Figure 17. For all of these abundance ratios, the values are virtually identical for all stars and show no difference with evolutionary state. As shown in Figure 17, these abundance ratios match the solar system *r*-process very well, and show no signs of varying with evolution. There are some offsets, with the most noticeable exceptions being Zr and Ba. We conclude that a large majority of all of the neutron-capture elements in M5 were synthesized in the *r*-process. Figure 16 shows how this can be contrasted with the globular cluster M4, which exhibits significant *s*-process contributions to its neutron-capture elements, even though it is roughly the same metallicity as M5 (Ivans et al. 1999; Yong et al. 2008a).

5.3.1. Age

In Figures 16 and 17, Th is low relative to the solar-system *r*-process value, as expected because it is radioactively unstable. This phenomenon allows us to date the stars in our sample based on their $\log \epsilon(\text{Th}/\text{Eu})$ values because Eu is a stable *r*-process element (e.g., Westin et al. 2000; Johnson & Bolte 2001; Ivans et al. 2006; Frebel et al. 2007). Using an initial *r*-process production ratio of $\log \epsilon(\text{Th}/\text{Eu}) = -0.28$ (Kratz et al. 2007), we determine an average age of 12.8 Gyr ($\sigma = 2.1$ Gyr) for the four stars with a (Th/Eu) abundance ratio measurement.

We find Th abundances lower than those reported by Yong et al. (2008a) for a different M5 sample. Using their $\log \epsilon(\text{Th}/\text{Eu})$ values, we determine an average cluster age of only 4.2 Gyr. Deriving ages from a (Th/Eu)

ratio can be problematic, however, as this ratio can sometimes be elevated in *r*-process-enhanced metal-poor stars (e.g., Figure 24 in Lai et al. 2008). An abundance variation in $\log \epsilon(\text{Th}/\text{Eu})$ in M5, though unlikely, may be one reason for this difference. Another possible cause for the difference could be in the adopted linelist. However, we use the same *gf* value for the 5989 Å Th II line as Yong et al. (2008a), and it is a fairly isolated line. It is possible there are unidentified features that could affect the synthesis, Aoki et al. (2007) point out a Nd II line in this region. Including this line, though, did not affect our results.

Our age determination of 12.8 Gyrs is about 1-3 Gyrs older than other estimates for the age of M5 based on CMD fitting (Meissner & Weiss 2006). However, given the caveats of using Th as an age indicator, and using $\sigma = 2.1$ Gyr as an estimate of our error, the Th age result is in reasonable agreement with these independent measurements.

5.3.2. Signs of the *s*-process

The heightened [Zr/Eu] and [Ba/Eu] ratios seen in our analysis may indicate an additional nucleosynthetic contribution from the *s*-process to the stars in M5. For Zr, a partial explanation of our results may come from comparing the abundances derived from the ionized species versus those from the neutral species (Table 7). For the three stars where both are measured, the neutral state gives an abundance ratio approximately 0.3 dex lower than the ionized state. This may indicate some systematic abundance analysis problems with Zr (e.g., as discussed in Section 5.1). Furthermore, interpreting the light neutron-capture elements including Zr (also Sr, Y, and Mo) is complicated by the possibility that they can have other nucleosynthetic contributions in addition to the main *s*-process (Snedden et al. 2008), including the weak *s*-process (Pignatari et al. 2010), charged particle reactions (Qian & Wasserburg 2008), and a light-element primary process (Travaglio et al. 2004).

However, the high measured [Zr/Eu] and [Ba/Eu] abundance ratios would fit the findings of an *s*-process contribution in Yong et al. (2008a,b) for their sample of two M5 RGB stars. In Figure 17, the nearly constant [Ba/Eu] and [La/Eu] over all evolutionary states indicate that this is not from an early onset of *s*-process material being dredged up in these AGB stars. Closer inspection of Figure 17 does show an intriguing trend where some of the elements are slightly elevated relative to the *r*-process-only line, although at lesser degrees than Zr and Ba.

We explore this in more detail in Table 12, where we present the average [X/Eu] abundance ratios of our sample along with the solar system *r*-process [X/Eu] ratio and percentage contribution to the solar system abundance from the *r*-process (Simmerer et al. 2004). All elements that can have a significant contribution from the *s*-process (> 70% in the solar system: Sr, Zr, Ba, La, and Ce, with the light-neutron capture elements Y and Mo being the only exceptions) are elevated in their [X/Eu] abundance ratio in M5 relative to the solar-system *r*-process [X/Eu]. On the other hand, the elements that can have a significant contribution from the *r*-process (> 30% in the solar system) fall almost exactly on the solar system *r*-process [X/Eu] value in M5 (Pr, Nd, Sm,

and Dy).

While clearly not *s*-process-dominated like the globular cluster M4, our derived abundances are an indication that there was some *s*-process material produced by an early generation of stars that contributed to the heavy element content of M5. These stars may have either formed within M5 and caused cluster self-enrichment, or formed before M5 and pre-enriched the gas that eventually became incorporated into its protocluster. While the overall scatter in each neutron-capture element abundance ratio relative to Eu is very low, we can test if this low scatter is tied to the light-element abundance variations. Figure 18 reproduces Figure 17, but with $[X/Eu]$ versus $[Na/Fe]$. It is clear from this plot that there is no correlation of $[X/Eu]$ with $[Na/Fe]$. Combined with the uniformity of the neutron-capture signature in the sample, this suggests that the *s*-process enhancements came from the protocluster gas, and not from cluster self-enrichment. As Yong et al. (2008b) point out, intermediate-mass AGB (IM-AGB) stars (in the mass range that experiences hot bottom burning) will produce very little to no *s*-process (Lattanzio et al. 2004), making it possible that they polluted the protocluster gas.

The sensitivity of the main *s*-process production to AGB-star mass could be linked to the existence of a smaller amount of *s*-process material in M5 compared to M4. In the M5 protocluster the mass function of pre-enriching AGB stars may not have extended to as low a mass as for the M4 protocluster, with the consequence that *s*-processing from AGB stars did not contribute as much to M5 as to M4. Such a circumstance might correlate with M5 being an outer halo globular cluster, while M4 has Galactic thick-disk-like kinematics. If M5 formed at an earlier time in Galactic history than M4, then less of a contribution could have been made to its element enrichment by the lowest mass IM-AGB stars. Alternatively, M5 may have formed in an *s*-process-poor dwarf “galaxy” that was acquired into the Galactic halo at a very early time in Galactic history, whereas M4 formed from the more chemically evolved proto-thick-disk. How common $[s\text{-process}/Fe]$ variations are, and the level to which they are present in other *r*-process-dominated clusters, would provide an important observational constraint to such scenarios.

The important caveat to this interpretation are the potential systematic offsets that may affect our abundance ratios as discussed in Section 5.1. There is a slight trend with $\log g$ in the $[Y/Eu]$ and $[Ba/Eu]$ abundance. The level of the trends, however, does not affect the above interpretation. Also, at least when comparing our neutron-capture abundances relative to Eu, there appears to be no offsets between stars of different stellar evolutionary stages in our investigation. We could, however, assume that the 0.15 dex offset found in our $[V/Fe]$ measurements also uniformly affects all of our $[X/Eu]$ determinations. A decrease in the average $[La/Eu]$ and $[Ce/Eu]$ ratios by this amount would allow these elements to be attributed to a pure *r*-process. However, it would still be necessary to explain the excess $[Ba/Eu]$ values, and we would have to assume that none of the other neutron-capture $[X/Eu]$ values are affected by this offset in a similar way.

6. CONCLUSIONS

We have performed detailed abundance analyses for a sample of evolved stars in the globular cluster M5, covering the RGB, RHB, and AGB branches of the CMD. Our conclusions can be broken into three parts.

The first is a cautionary note. It appears that there can be systematic abundance offsets induced when analyzing stars on the different evolutionary branches using standard onedimensional LTE abundance analysis and atmospheres. This can manifest itself not only in absolute abundances, but more worryingly in abundance ratios such as $[Ca/Fe]$. The largest offset found was in $[V/Fe]$, with a 0.15 dex difference between the AGB versus RGB stars. This puts a limit on how well abundances among the different evolutionary branches of M5 can be compared.

The second conclusion is that our sample clearly shows the signatures of star-to-star abundance differences related to the CNO, Ne–Na, and Mg–Al nuclear reaction cycles, and that there are no discernible differences in these element patterns with stellar evolution phase. This agrees with theoretical predictions that self-pollution and mixing within present-day globular cluster stars will not begin until the thermal pulsation phase of the AGB. Taking this into context with the M5 turn-off stars analyzed in Ramírez & Cohen (2003), the (N-,Na-,Al)-rich cluster stars are present throughout all post-main-sequence phases of evolution. This is consistent with such stars having acquired their surface element enhancements from external sources, and not from the outwards transport of material processed through H-burning reactions within their interiors.

The third conclusion is that we find the neutron-capture abundances of M5 to be *r*-process dominated, but with what we interpret as a small uniform addition of *s*-process material. This neutron-capture signature is constant through all stars in our sample, depending on neither evolution nor the light-element variations. This suggests that low-mass AGB stars contributed heavy elements to the primordial cluster environment. However, the lack of correlation with the light-element variations also seems to preclude low-mass AGB stars from having much of a contribution once star formation had begun.

D.K.L acknowledges the support of the National Science Foundation through the NSF Astronomy and Astrophysics Postdoctoral Fellowship under award AST-0802292.

G.H.S. acknowledges support from NSF grant AST-0406988. M. B. and J. A. J. acknowledges support from NSF grant AST-0607770 and AST-0607482. S.L. is grateful to the DFG cluster of excellence “Origin and Structure of the Universe” for partial support. We thank the anonymous referee whose careful reading and suggestions helped improve the paper.

Facility: Keck:I (HIRES)

REFERENCES

- Aldenius, M., Tanner, J. D., Johansson, S., Lundberg, H., & Ryan, S. G. 2007, *A&A*, 461, 767
- Anders, E., & Grevesse, N. 1989, *Geochim. Cosmochim. Acta*, 53, 197
- Aoki, W., Honda, S., Sadakane, K., & Arimoto, N. 2007, *PASJ*, 59, L15

- Arlandini, C., Käppeler, F., Wisshak, K., Gallino, R., Lugaro, M., Busso, M., & Straniero, O. 1999, *ApJ*, 525, 886
- Arp, H. C. 1955, *AJ*, 60, 317
- Asplund, M. 2005, *ARA&A*, 43, 481
- Asplund, M., Grevesse, N., Sauval, A. J., & Scott, P. 2009, *ARA&A*, 47, 481
- Baumüller, D., Butler, K., & Gehren, T. 1998, *A&A*, 338, 637
- Baumüller, D., & Gehren, T. 1997, *A&A*, 325, 1088
- Behr, B. B., Cohen, J. G., & McCarthy, J. K. 2000, *ApJ*, 531, L37
- Bragaglia, A., et al. 2010, *ApJ*, 720, L41
- Briley, M. M., Smith, G. H., Bell, R. A., Oke, J. B., & Hesser, J. E. 1992, *ApJ*, 387, 612
- Brown, J. A., & Wallerstein, G. 1989, *AJ*, 98, 1643
- Buonanno, R., Corsi, C. E., & Fusi Pecci, F. 1981, *MNRAS*, 196, 435
- Busso, M., Palmerini, S., Maiorca, E., Cristallo, S., Straniero, O., Abia, C., Gallino, R., & La Cognata, M. 2010, *ApJ*, 717, L47
- Busso, M., Wasserburg, G. J., Nollett, K. M., & Calandra, A. 2007, *ApJ*, 671, 802
- Campbell, S. W., Lattanzio, J. C., & Elliott, L. M. 2006, *Memorie della Societa Astronomica Italiana*, 77, 864
- Campbell, S. W., Yong, D., Wylie-de Boer, E. C., Stancliffe, R. J., Lattanzio, J. C., Angelou, G. C., Grundahl, F., & Sneden, C. 2010, *ArXiv e-prints*
- Carretta, E., Bragaglia, A., Gratton, R., D'Orazi, V., & Lucatello, S. 2009a, *A&A*, 508, 695
- Carretta, E., Bragaglia, A., Gratton, R., & Lucatello, S. 2009b, *A&A*, 505, 139
- Carretta, E., Bragaglia, A., Gratton, R., Lucatello, S., Bellazzini, M., & D'Orazi, V. 2010a, *ApJ*, 712, L21
- Carretta, E., et al. 2009c, *A&A*, 505, 117
- Carretta, E., Bragaglia, A., Gratton, R. G., Recio-Blanco, A., Lucatello, S., D'Orazi, V., & Cassisi, S. 2010b, *A&A*, 516, A55+
- Carretta, E., Gratton, R. G., Bragaglia, A., Bonifacio, P., & Pasquini, L. 2004, *A&A*, 416, 925
- Castelli, F. 2005, *Memorie della Societa Astronomica Italiana Supplement*, 8, 34
- Charbonnel, C., & Zahn, J. 2007, *A&A*, 467, L15
- Clement, C. M., & Shelton, I. 1997, *AJ*, 113, 1711
- Cohen, J. G., Briley, M. M., & Stetson, P. B. 2002, *AJ*, 123, 2525
- Cottrell, P. L., & Da Costa, G. S. 1981, *ApJ*, 245, L79
- de Mink, S. E., Pols, O. R., Langer, N., & Izzard, R. G. 2009, *A&A*, 507, L1
- Decressin, T., Meynet, G., Charbonnel, C., Prantzos, N., & Ekström, S. 2007, *A&A*, 464, 1029
- Denissenkov, P. A. 2010, *ApJ*, 723, 563
- Denissenkov, P. A., Pinsonneault, M., & MacGregor, K. B. 2009, *ApJ*, 696, 1823
- D'Orazi, V., & Marino, A. F. 2010, *ApJ*, 716, L166
- Eggleton, P. P., Dearborn, D. S. P., & Lattanzio, J. C. 2006, *Science*, 314, 1580
- . 2008, *ApJ*, 677, 581
- Fitzpatrick, M. J., & Sneden, C. 1987, in *Bulletin of the American Astronomical Society*, Vol. 19, *Bulletin of the American Astronomical Society*, 1129+
- Frebel, A., Christlieb, N., Norris, J. E., Thom, C., Beers, T. C., & Rhee, J. 2007, *ApJ*, 660, L117
- Fuhr, J. R., & Wiese, W. L. 2006, *Journal of Physical and Chemical Reference Data*, 35, 1669
- Gratton, R. G., et al. 2001, *A&A*, 369, 87
- Gratton, R. G., Carretta, E., Eriksson, K., & Gustafsson, B. 1999, *A&A*, 350, 955
- Gratton, R. G., Sneden, C., Carretta, E., & Bragaglia, A. 2000, *A&A*, 354, 169
- Griest, K., Whitmore, J. B., Wolfe, A. M., Prochaska, J. X., Howk, J. C., & Marcy, G. W. 2010, *ApJ*, 708, 158
- Gustafsson, B., Edvardsson, B., Eriksson, K., Jørgensen, U. G., Nordlund, Å., & Plez, B. 2008, *A&A*, 486, 951
- Harris, W. E. 1996, *AJ*, 112, 1487
- Hesser, J. E., Hartwick, F. D. A., & McClure, R. D. 1977, *ApJS*, 33, 471
- Hoppe, P., Annen, P., Strebler, R., Eberhardt, P., Gallino, R., Lugaro, M., Amari, S., & Lewis, R. S. 1997, *ApJ*, 487, L101+
- Houdashelt, M. L., Bell, R. A., & Sweigart, A. V. 2000, *AJ*, 119, 1448
- Ivans, I. I., Kraft, R. P., Sneden, C., Smith, G. H., Rich, R. M., & Shetrone, M. 2001, *AJ*, 122, 1438
- Ivans, I. I., Simmerer, J., Sneden, C., Lawler, J. E., Cowan, J. J., Gallino, R., & Bisterzo, S. 2006, *ApJ*, 645, 613
- Ivans, I. I., Sneden, C., James, C. R., Preston, G. W., Fulbright, J. P., Höflich, P. A., Carney, B. W., & Wheeler, J. C. 2003, *ApJ*, 592, 906
- Ivans, I. I., Sneden, C., Kraft, R. P., Suntzeff, N. B., Smith, V. V., Langer, G. E., & Fulbright, J. P. 1999, *AJ*, 118, 1273
- Johnson, J. A. 2002, *ApJS*, 139, 219
- Johnson, J. A., & Bolte, M. 2001, *ApJ*, 554, 888
- Kaluzny, J., Olech, A., Thompson, I., Pych, W., Krzeminski, W., & Schwarzenberg-Czerny, A. 2000, *A&AS*, 143, 215
- Karakas, A. I., Campbell, S. W., & Stancliffe, R. J. 2010, *ApJ*, 713, 374
- Keller, L. D., Pilachowski, C. A., & Sneden, C. 2001, *AJ*, 122, 2554
- Kippenhahn, R., Ruschenplatt, G., & Thomas, H. 1980, *A&A*, 91, 175
- Kirby, E. N., Guhathakurta, P., Bolte, M., Sneden, C., & Geha, M. C. 2009, *ApJ*, 705, 328
- Koch, A., & McWilliam, A. 2008, *AJ*, 135, 1551
- . 2010, *AJ*, 139, 2289
- Korn, A. J., Grundahl, F., Richard, O., Mashonkina, L., Barklem, P. S., Collet, R., Gustafsson, B., & Piskunov, N. 2007, *ApJ*, 671, 402
- Kraft, R. P. 1994, *PASP*, 106, 553
- Kraft, R. P., & Ivans, I. I. 2003, *PASP*, 115, 143
- Kratz, K.-L., Farouqi, K., Pfeiffer, B., Truran, J. W., Sneden, C., & Cowan, J. J. 2007, *ApJ*, 662, 39
- Kurucz, R. 1993, *ATLAS9 Stellar Atmosphere Programs and 2 km/s grid*. Kurucz CD-ROM No. 13. Cambridge, Mass.: Smithsonian Astrophysical Observatory, 1993., 13
- Kurucz, R. L., & Bell, B. 1995, *Atomic line list (Kurucz CD-ROM, Cambridge, MA: Smithsonian Astrophysical Observatory, —c1995, April 15, 1995)*
- Lai, D. K., Bolte, M., Johnson, J. A., Lucatello, S., Heger, A., & Woosley, S. E. 2008, *ApJ*, 681, 1524
- Lambert, D. L., Gustafsson, B., Eriksson, K., & Hinkle, K. H. 1986, *ApJS*, 62, 373
- Langer, G. E., Kraft, R. P., & Friel, E. D. 1985, *PASP*, 97, 373
- Lattanzio, J., Karakas, A., Campbell, S., Elliott, L., & Chieffi, A. 2004, *Mem. Soc. Astron. Italiana*, 75, 322
- Lawler, J. E., Bonvallet, G., & Sneden, C. 2001a, *ApJ*, 556, 452
- Lawler, J. E., Wickliffe, M. E., den Hartog, E. A., & Sneden, C. 2001b, *ApJ*, 563, 1075
- Lebzelter, T., Lederer, M. T., Cristallo, S., Hinkle, K. H., Straniero, O., & Aringer, B. 2008, *A&A*, 486, 511
- Lee, J., Kang, Y., Lee, J., & Lee, Y. 2009, *Nature*, 462, 480
- Ljung, G., Nilsson, H., Asplund, M., & Johansson, S. 2006, *A&A*, 456, 1181
- Lodders, K., Plame, H., & Gail, H. 2009, in *Landolt-Börnstein - Group VI Astronomy and Astrophysics Numerical Data and Functional Relationships in Science and Technology Volume 4B: Solar System*. Edited by J.E. Trümper, 2009, 4.4., 44+
- Lucatello, S., Gratton, R., Cohen, J. G., Beers, T. C., Christlieb, N., Carretta, E., & Ramírez, S. 2003, *AJ*, 125, 875
- Mashonkina, L. I., Shimanskiĭ, V. V., & Sakhিবullin, N. A. 2000, *Astronomy Reports*, 44, 790
- Masseron, T., et al. 2006, *A&A*, 455, 1059
- McWilliam, A. 1998, *AJ*, 115, 1640
- Meissner, F., & Weiss, A. 2006, *A&A*, 456, 1085
- Milam, S. N., Woolf, N. J., & Ziurys, L. M. 2009, *ApJ*, 690, 837
- Mucciarelli, A., Origlia, L., Ferraro, F. R., & Pancino, E. 2009, *ApJ*, 695, L134
- Nilsson, H., Ljung, G., Lundberg, H., & Nielsen, K. E. 2006, *A&A*, 445, 1165
- Nilsson, H., Zhang, Z. G., Lundberg, H., Johansson, S., & Nordström, B. 2002, *A&A*, 382, 368
- Norris, J., Cottrell, P. L., Freeman, K. C., & Da Costa, G. S. 1981, *ApJ*, 244, 205
- Norris, J., & Smith, G. H. 1983, *ApJ*, 272, 635
- Osborn, W. 1971, *The Observatory*, 91, 223
- Pavlenko, Y. V., Jones, H. R. A., & Longmore, A. J. 2003, *MNRAS*, 345, 311

- Pignatari, M., Gallino, R., Heil, M., Wiescher, M., Käppeler, F., Herwig, F., & Bisterzo, S. 2010, *ApJ*, 710, 1557
- Pike, C. D. 1978, *MNRAS*, 183, 101
- Qian, Y., & Wasserburg, G. J. 2008, *ApJ*, 687, 272
- Ralchenko, Y., Kramida, A. E., Reader, J., & NIST ASD Team. 2008, NIST Atomic Spectra Database (v. 3.1.5), <http://physics.nist.gov/asd3>
- Ramírez, I., & Meléndez, J. 2005, *ApJ*, 626, 465
- Ramírez, S. V., & Cohen, J. G. 2003, *AJ*, 125, 224
- Recio-Blanco, A., & de Laverny, P. 2007, *A&A*, 461, L13
- Sandquist, E. L., & Bolte, M. 2004, *ApJ*, 611, 323
- Sandquist, E. L., Bolte, M., Stetson, P. B., & Hesser, J. E. 1996, *ApJ*, 470, 910
- Scholz, R., Odenkirchen, M., Hirte, S., Irwin, M. J., Borngen, F., & Ziener, R. 1996, *MNRAS*, 278, 251
- Shetrone, M. D. 2003, *ApJ*, 585, L45
- Shi, J. R., Gehren, T., & Zhao, G. 2004, *A&A*, 423, 683
- Simmerer, J., Sneden, C., Cowan, J. J., Collier, J., Woolf, V. M., & Lawler, J. E. 2004, *ApJ*, 617, 1091
- Simoda, M., & Tanikawa, K. 1970, *PASJ*, 22, 143
- Skrutskie, M. F., et al. 2006, *AJ*, 131, 1163
- Smith, G. H., & Martell, S. L. 2003, *PASP*, 115, 1211
- Smith, G. H., & Norris, J. E. 1993, *AJ*, 105, 173
- Smith, G. H., Shetrone, M. D., Briley, M. M., Churchill, C. W., & Bell, R. A. 1997, *PASP*, 109, 236
- Sneden, C., Cowan, J. J., & Gallino, R. 2008, *ARA&A*, 46, 241
- Sneden, C., et al. 2003, *ApJ*, 591, 936
- Sneden, C., Ivans, I. I., & Kraft, R. P. 2000, *Memorie della Societa Astronomica Italiana*, 71, 657
- Sneden, C., Kraft, R. P., Prosser, C. F., & Langer, G. E. 1992, *AJ*, 104, 2121
- Sneden, C., Kraft, R. P., Shetrone, M. D., Smith, G. H., Langer, G. E., & Prosser, C. F. 1997, *AJ*, 114, 1964
- Sneden, C. A. 1973, PhD thesis, AA(THE UNIVERSITY OF TEXAS AT AUSTIN.)
- Sobeck, J. S., Ivans, I. I., Simmerer, J. A., Sneden, C., Hoefflich, P., Fulbright, J. P., & Kraft, R. P. 2006, *AJ*, 131, 2949
- Sobeck, J. S., Lawler, J. E., & Sneden, C. 2007, *ApJ*, 667, 1267
- Stancliffe, R. J. 2010, *MNRAS*, 403, 505
- Thévenin, F., & Idiart, T. P. 1999, *ApJ*, 521, 753
- Travaglio, C., Gallino, R., Arnone, E., Cowan, J., Jordan, F., & Sneden, C. 2004, *ApJ*, 601, 864
- Ventura, P., & D'Antona, F. 2009, *A&A*, 499, 835
- Vogt, S. S., et al. 1994, in Presented at the Society of Photo-Optical Instrumentation Engineers (SPIE) Conference, Vol. 2198, Proc. SPIE Instrumentation in Astronomy VIII, David L. Crawford; Eric R. Craine; Eds., Volume 2198, p. 362, ed. D. L. Crawford & E. R. Craine, 362–+
- Westin, J., Sneden, C., Gustafsson, B., & Cowan, J. J. 2000, *ApJ*, 530, 783
- Yong, D., Karakas, A. I., Lambert, D. L., Chieffi, A., & Limongi, M. 2008a, *ApJ*, 689, 1031
- Yong, D., Lambert, D. L., Paulson, D. B., & Carney, B. W. 2008b, *ApJ*, 673, 854
- Zinn, R. 1977, *ApJ*, 218, 96

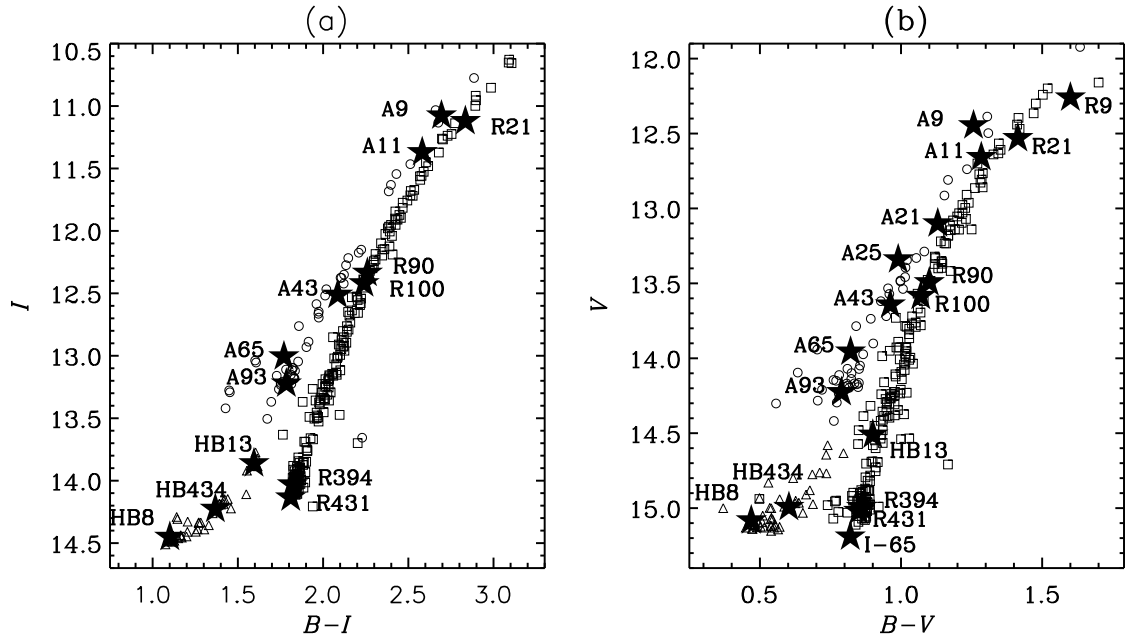


Figure 1. CMD of M5 in two different colors: (a) $B-I$ and (b) $B-V$. The circles correspond to AGB stars, the triangles to HB stars, and the squares to RGB stars. The stars included in our HIRES observational sample are plotted with the filled star symbols.

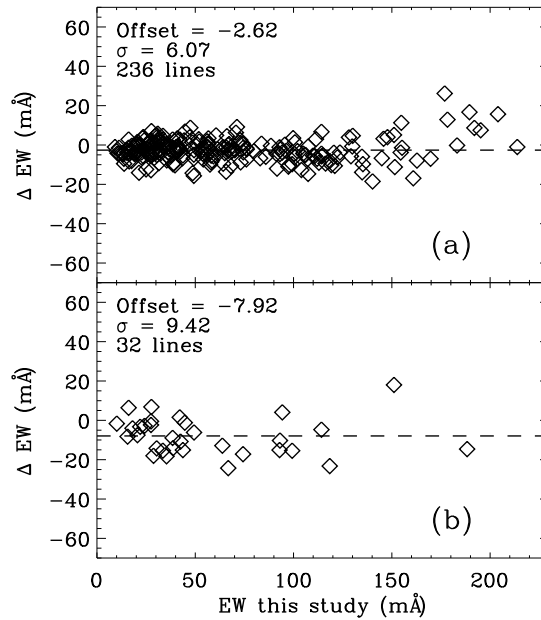


Figure 2. (a) Comparison of EWs measured by our study and Ramírez & Cohen (2003). Plotted are the differences between the EWs, in the sense of our study minus Ramírez & Cohen (2003), vs. the EWs from our study. (b) Comparison of EWs measured by our study and Ivans et al. (2001). The EWs from Ivans et al. (2001) originally come from Sneden et al. (1992), and have been transformed to their Keck scale. The difference ΔEW is in the sense of our study minus Ivans et al. (2001).

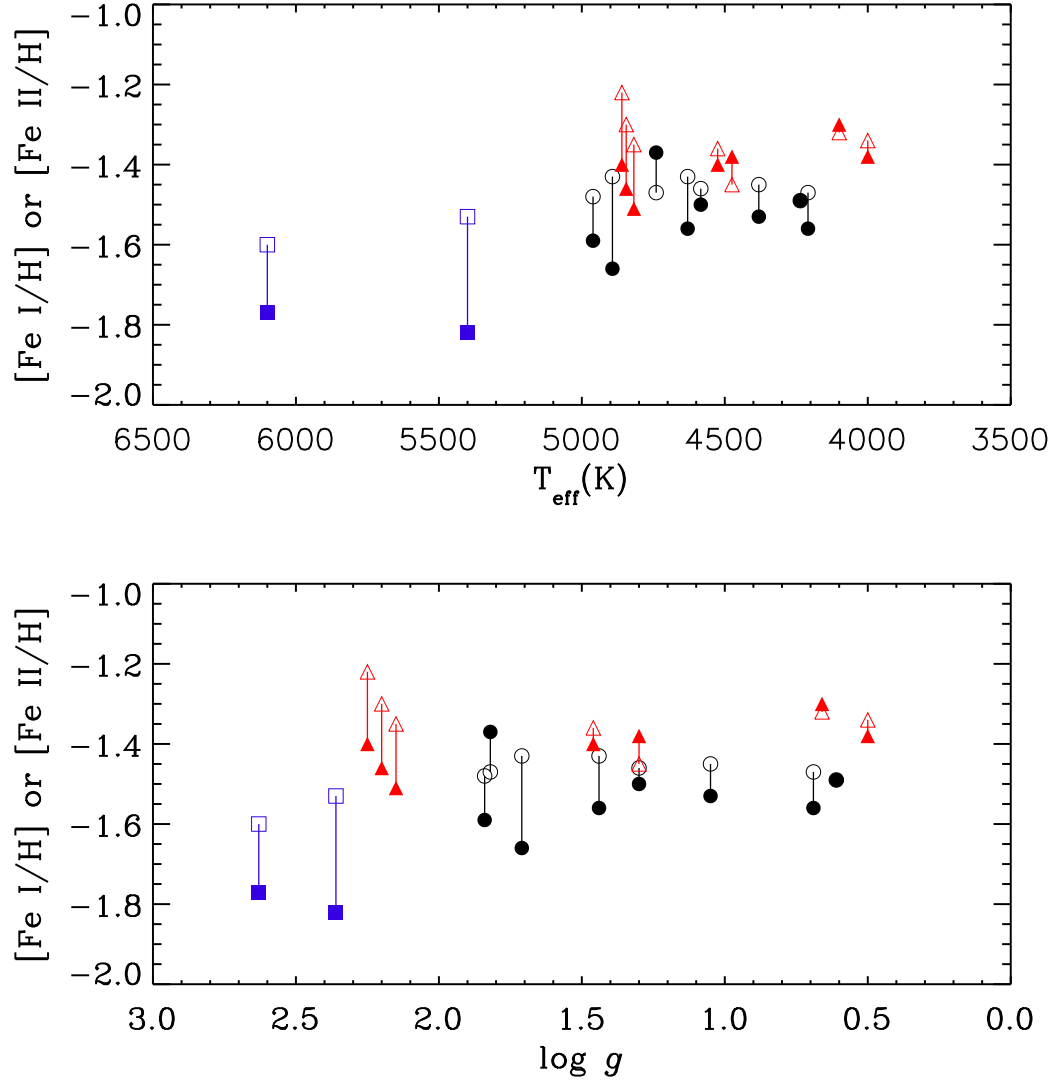


Figure 3. Our measurements of [Fe I/H] (solid symbols) and [Fe II/H] (hollow symbols) vs. effective temperature and surface gravity. The circles correspond to AGB stars, the triangles to RGB stars, and the squares to HB stars (colored black, red, and blue, respectively in the electronic edition). The lines connect the [Fe I/H] and [Fe II/H] measurements from the same star. In most of the stars, [Fe I/H] is lower than [Fe II/H]. There is also an offset of both the [Fe I/H] and [Fe II/H] between different evolutionary states.

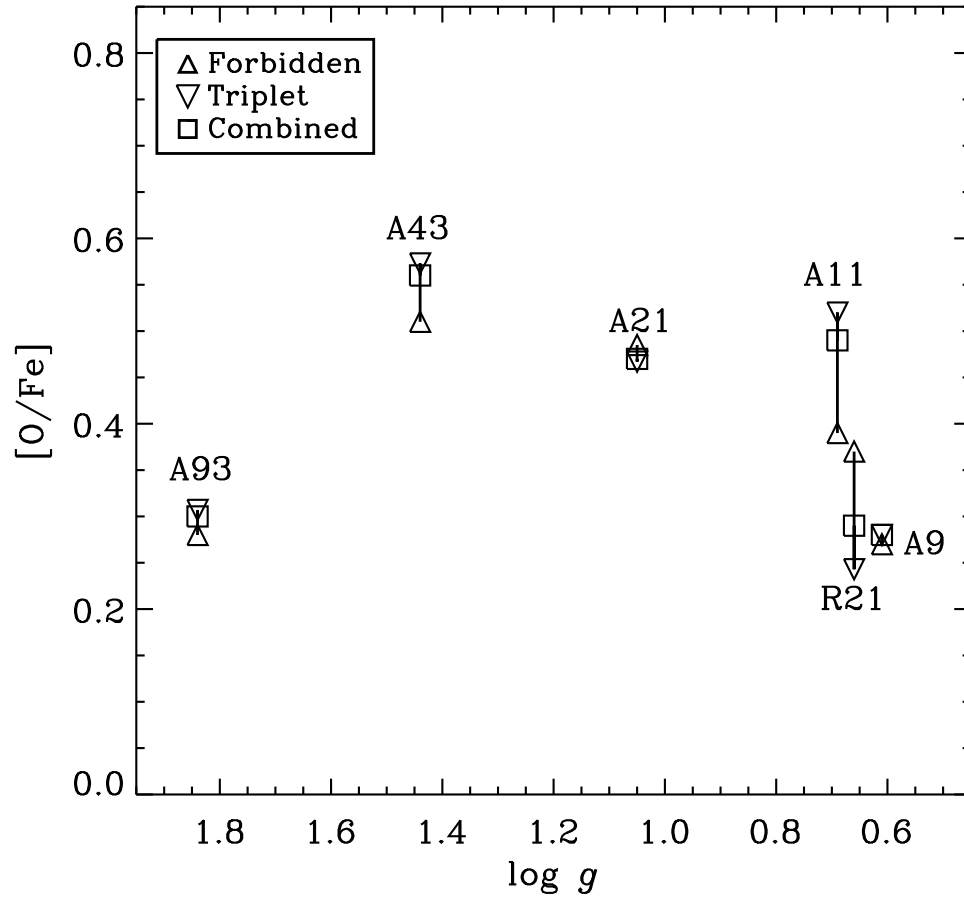


Figure 4. In six of our stars both forbidden and triplet lines of O were measured. Plotted are $[O/Fe]$ derived individually from both sets of lines, along with the final combined abundance value vs. stellar surface gravity. A solid line connects the measurements for each individual star. Note that the combined $[O/Fe]$ is not the average of the forbidden and triplet values because there are different number of lines coming from each set (see Table 2).

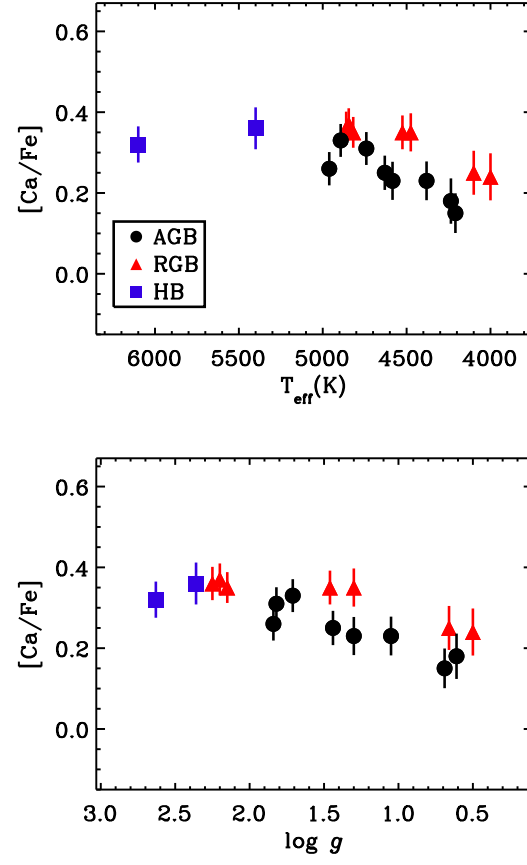


Figure 5. Our values of $[\text{Ca}/\text{Fe}]$ plotted against $\log g$ and T_{eff} . There is an offset in $[\text{Ca}/\text{Fe}]$ of ~ 0.08 dex between the AGB and RGB stars.

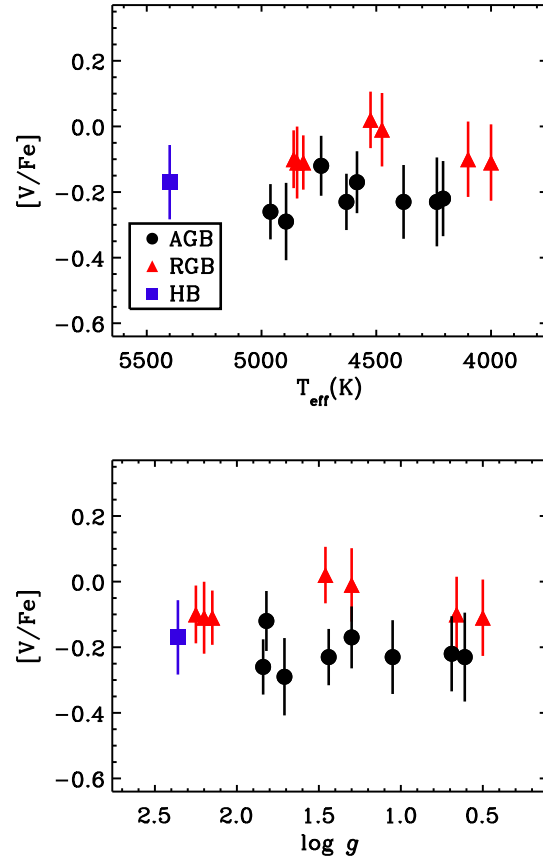


Figure 6. Our values of $[V/Fe]$ plotted against $\log g$ and T_{eff} . Like with $[Ca/Fe]$, there is an offset between the AGB and RGB stars, but in this case it is 0.15 dex.

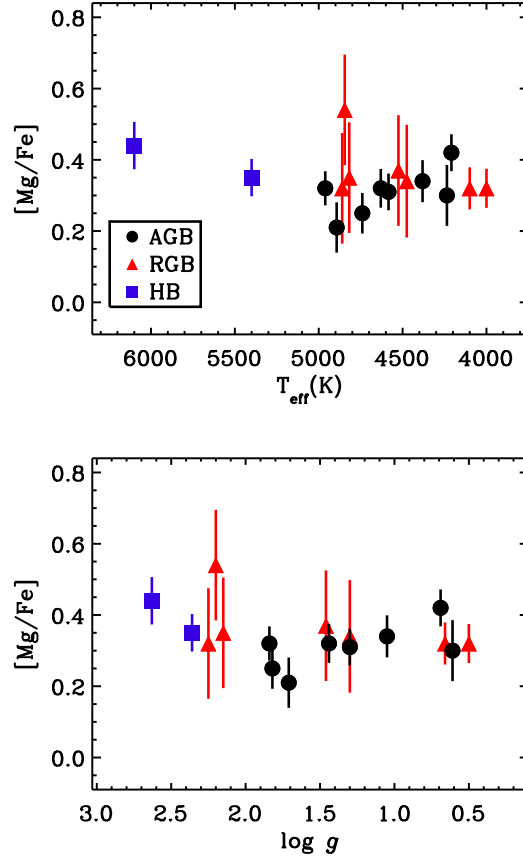


Figure 7. Our values of $[Mg/Fe]$ plotted against $\log g$ and T_{eff} . Within the errors, all of the stars are consistent with a constant $[Mg/Fe]$ value of 0.34.

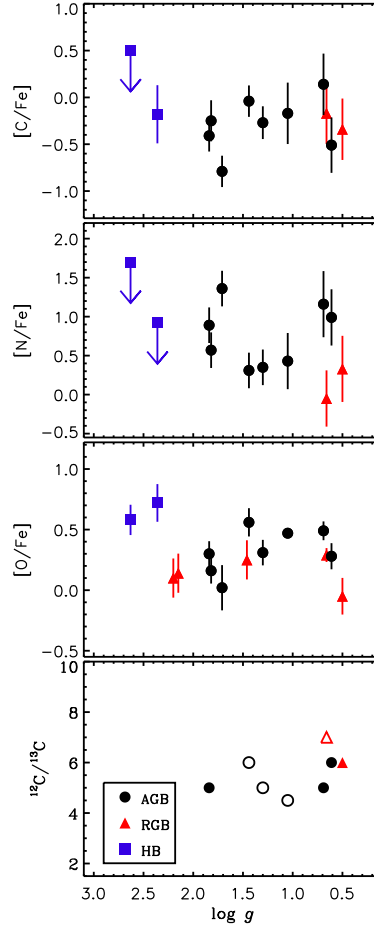


Figure 8. $[\text{C}/\text{Fe}]$, $[\text{N}/\text{Fe}]$, $[\text{O}/\text{Fe}]$, and $^{12}\text{C}/^{13}\text{C}$ vs. surface gravity for stars in our M5 sample. There does appear to be some variation of the derived $[\text{C}/\text{Fe}]$ abundance ratios. However with the large uncertainties, all but one of our stars is consistent with having $[\text{C}/\text{Fe}] \sim -0.2$. Among the AGB stars there is a notable variation in $[\text{N}/\text{Fe}]$. The comparison between the RGB stars and AGB stars for $[\text{N}/\text{Fe}]$ in our sample is hindered by the small number of the former, and possible systematic differences in the atmospheres of these two evolutionary groups. $[\text{O}/\text{Fe}]$ shows star-to-star variations, although not as large as with $[\text{N}/\text{Fe}]$. For the $^{12}\text{C}/^{13}\text{C}$ plot, the filled symbols represent stars with $[\text{Na}/\text{Fe}] \geq 0.15$, while the hollow symbols represent stars with $[\text{Na}/\text{Fe}] < 0.15$. While only able to measure the $^{12}\text{C}/^{13}\text{C}$ ratio for a handful of stars, we find that the results are all consistent with a value of ~ 5 . The error bars on all of the measurement are ± 2 . In particular, we find the same $^{12}\text{C}/^{13}\text{C}$ ratio in the RGB stars as in the AGB stars of our sample and that there is no difference in values in the Na-high vs. Na-low stars.

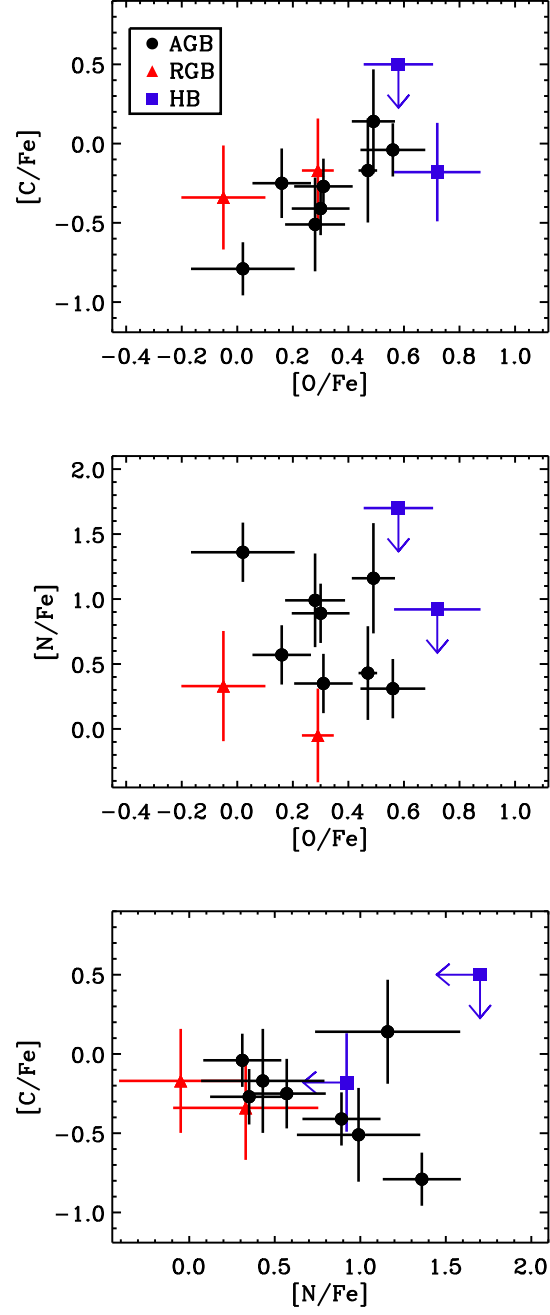


Figure 9. Relative behavior of the CNO abundances among the M5 sample. At least among the AGB stars, there appears a clear C–O correlation and C–N anticorrelation, although evidence for an O–N anticorrelation appears less secure. Such trends are signatures of the CNO cycle having affected the abundances of these stars.

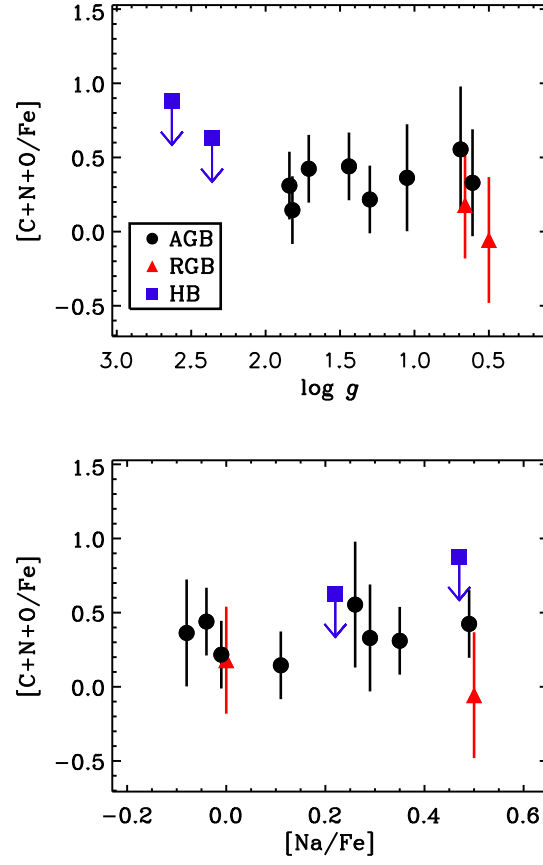


Figure 10. $[C+N+O/Fe]$ values are consistent with being constant for the stars in which it could be measured. The average for these stars is $\langle [C+N+O/Fe] \rangle = 0.37$.

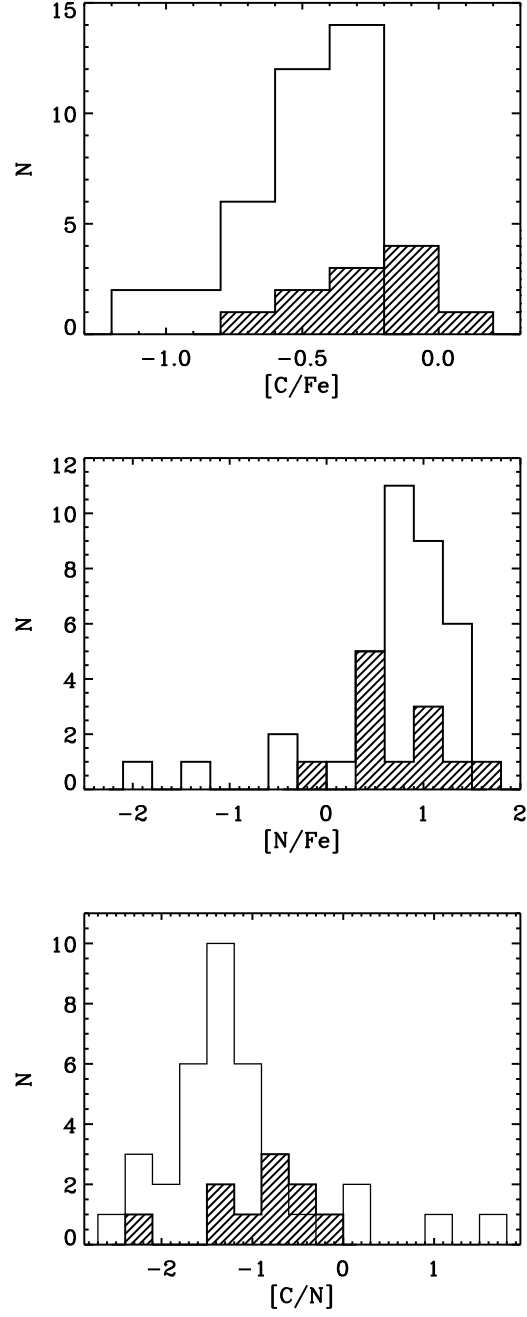


Figure 11. We show our $[C/Fe]$, $[N/Fe]$, and $[C/N]$ distribution as compared to the study of Cohen et al. (2002) for the same quantities. The filled histograms represent this work, and the empty histograms Cohen et al. (2002). For $[C/Fe]$ we choose a binning of 0.2 dex, while the binning is 0.3 dex for $[N/Fe]$ and $[C/N]$ due to the larger distribution of values in these latter two quantities.

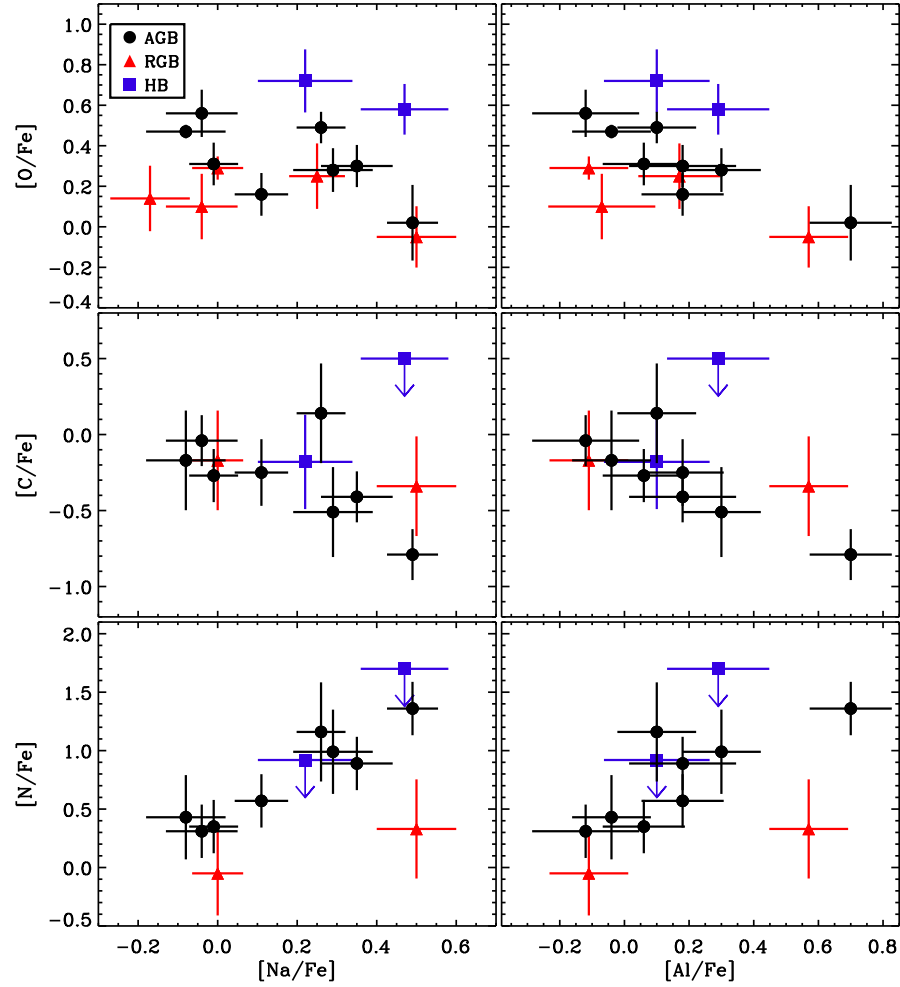


Figure 12. CNO abundances are shown plotted vs. $[\text{Na}/\text{Fe}]$ and $[\text{Al}/\text{Fe}]$. Our data are consistent with an O–Na and C–Na anticorrelation among the AGB stars, but inconclusive for the RGB and RHB stars. However, there is a reasonably strong N–Na correlation, with the caution that the data for the two RGB stars may be systematically offset from that for the AGB stars. Similar (anti)correlations are apparent for O–Al, C–Al, and N–Al. We note that for two of our stars, HB434 and HB8, $[\text{Al}/\text{Fe}]$ could only be derived from using the Al resonance lines at 3944 and 3962 Å. For these two stars, an NLTE correction is adopted from Baumüller & Gehren (1997) of +0.65 dex.

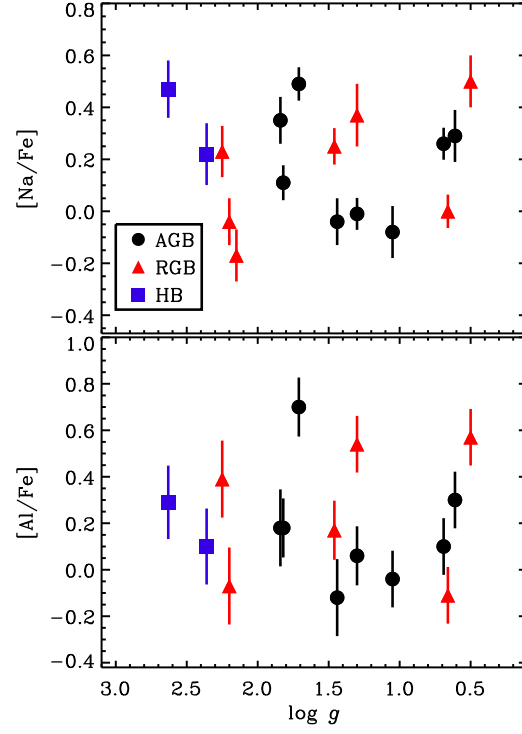


Figure 13. $[Na/Fe]$ and $[Al/Fe]$ abundances, shown here plotted vs. surface gravity, show no discernible trend with evolutionary state or atmospheric parameters.

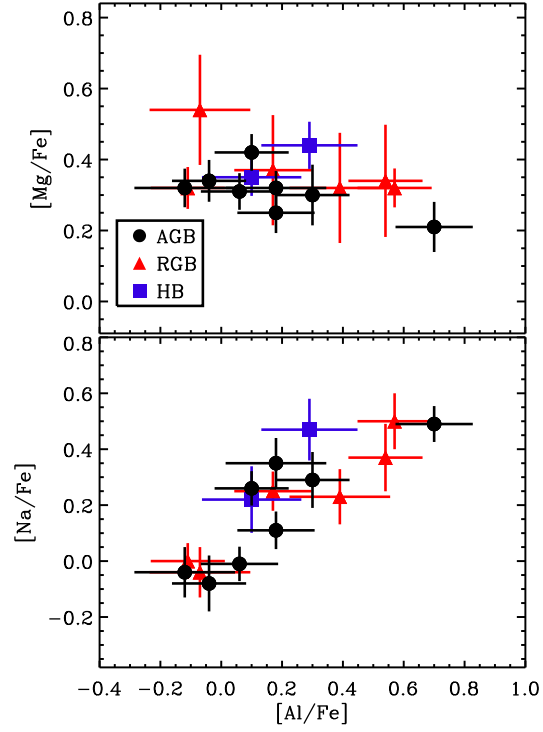


Figure 14. Relative behavior of both Mg and Na vs. Al abundance for the M5 sample. Two points at $[Al/Fe] = -0.1$ and $+0.7$ drive the possible appearance of an Mg–Al anticorrelation, but the Na–Al correlation is clear, with little or no offset among stars in different evolutionary states. For two of our stars, HB434 and HB8, $[Al/Fe]$ could only be derived from using the Al resonance lines at 3944 and 3962 Å. For these two stars, an NLTE correction is adopted from Baumueller & Gehren (1997) of $+0.65$ dex.

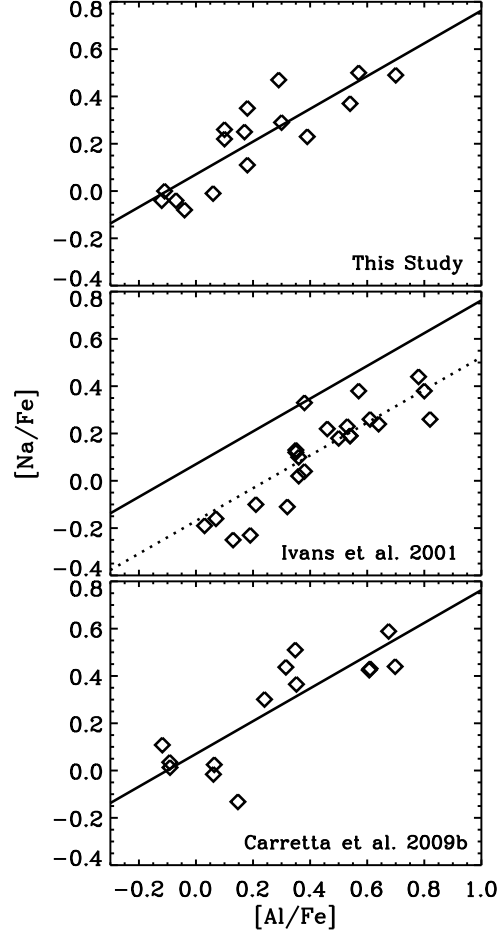


Figure 15. Na–Al correlation from this study is compared to those found by Ivans et al. (2001) and Carretta et al. (2009b). The solid line in each plot is the best-fit line to our Na–Al measurements, and matches fairly well the data points of Carretta et al. (2009b). The Ivans et al. (2001) data lie below our best-fit line; however, this can be almost completely accounted for by different adopted gf values for the measured Al transitions. Assuming the gf values from Ivans et al. (2001) would reduce our Al abundances by ~ 0.24 dex. Shifting our best-fit line by this amount gives the dotted line, which agrees very well with the trend seen in the Ivans et al. (2001) data.

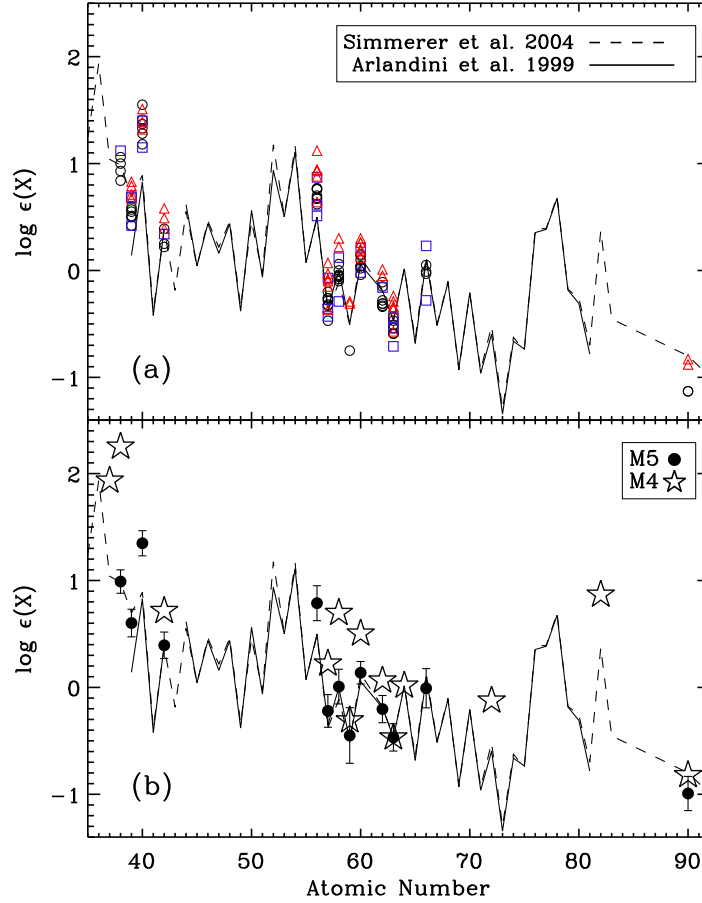


Figure 16. (a) Plotted are the measured neutron-capture element abundances vs. atomic number for all stars in our M5 sample. We overplot the solar system r -process abundance patterns from Arlandini et al. (1999) and Simmerer et al. (2004), scaled to our average $\log \epsilon(\text{Eu})$ value of -0.47 ($A = 63$). The Zr abundances represent both Zr I and Zr II. When both ionization states of Zr are measured in a star, the average of the two is plotted in this figure. The hollow triangles, hollow squares, and hollow circles correspond to RGB, HB, and AGB stars (red, blue, and black in the electronic edition), respectively. (b) This panel plots the average for each abundance measurement (solid circles). The error bars represent the standard deviation of the measured abundances. Also plotted are the average neutron-capture abundances from M4 as measured by Yong et al. (2008a) and Yong et al. (2008b), scaled to the average $\log \epsilon(\text{Eu})$ we measure for our M5 sample.

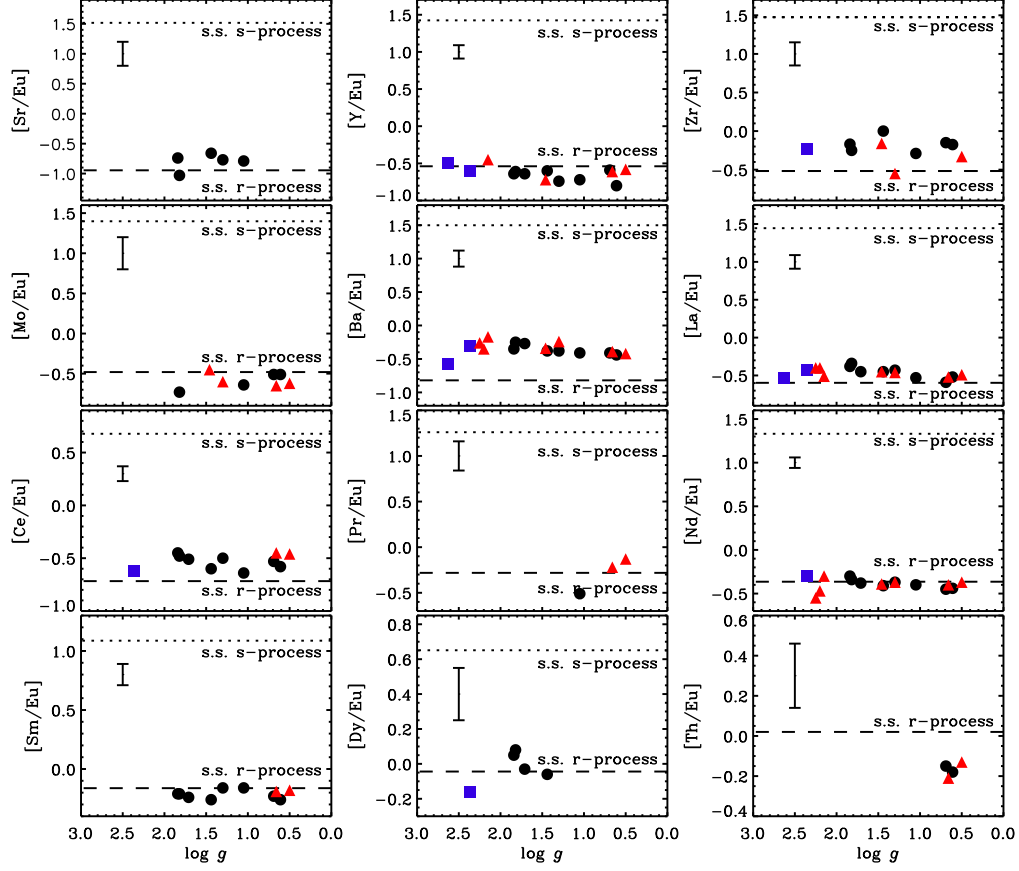


Figure 17. Heavy element to Eu ratios $[X/Eu]$ measured for the M5 stars in our sample vs. surface gravity. The r -process origin of the neutron-capture elements we measure is evident when we compare to the solar system r -process (dashed lines) and solar system s -process (dotted lines) ratios as derived from Simmerer et al. (2004). The symbols are as in Figure 5, i.e., triangles, squares, and circles correspond to RGB, HB, and AGB stars, respectively. A typical error bar is shown in the top left corner of each plot. The average values of $[X/Eu]$ and σ are given in Table 12.

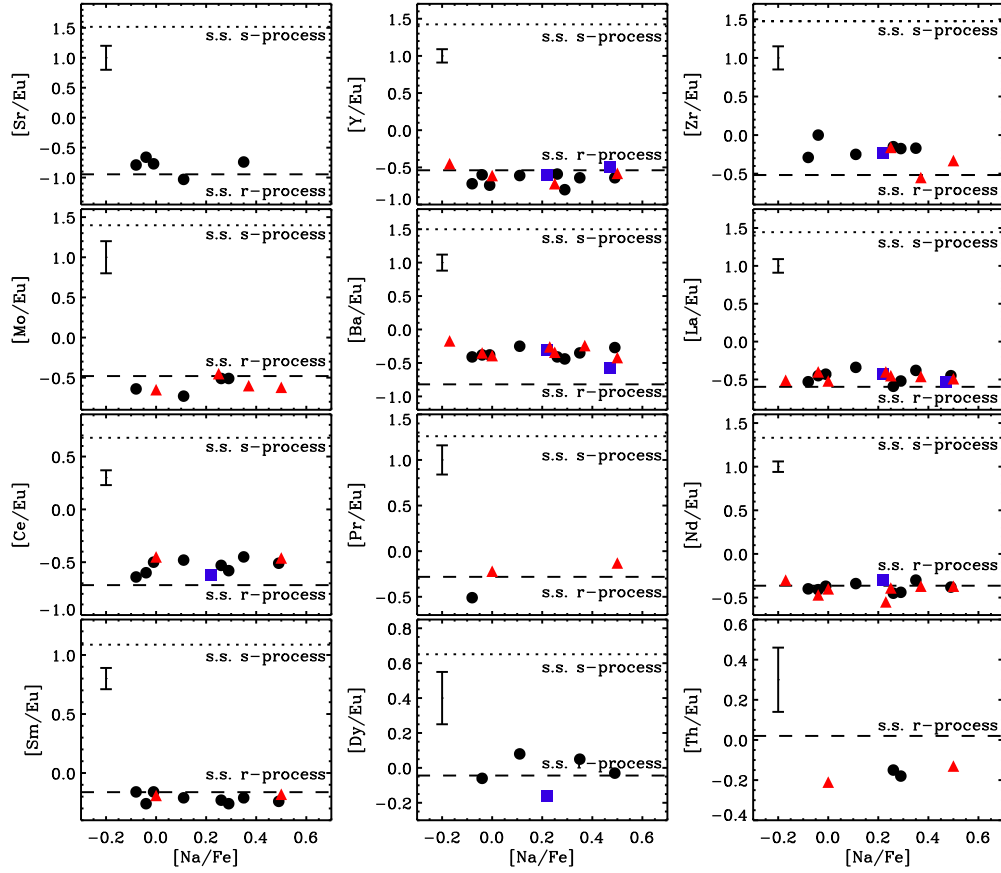


Figure 18. Heavy element to Eu ratios $[X/Eu]$ measured for the M5 stars in our sample vs. $[Na/Fe]$. A typical error bar is shown in the top left corner of each plot. The lack of correlation with evolution shown in Figure 17 persists when compared to the light-element variations such as $[Na/Fe]$.

Table 1
Observation Details

Name	Alt. Name	V (mag)	$B - V$ (mag)	Observing Run	Total Exp. (s)	S/N at 6035 Å	Evolutionary State
A9		12.45	1.26	2007 Jun	1200	142	AGB
A11	IV-59	12.66	1.28	2007 Jun	1980	123	AGB
A21	II-258	13.10	1.13	2007 Jun	1800	131	AGB
A25		13.34	0.99	2007 Jun	2100	115	AGB
A43		13.64	0.96	2007 Jun	2700	135	AGB
A65	I-67	13.96	0.82	2007 Jun	3600	104	AGB
A93		14.23	0.79	2007 Jun	5400	132	AGB
HB13		14.51	0.90	2007 Jun	5760	125	AGB
HB434		14.99	0.60	2007 Jun	7200	113	HB
HB8		15.08	0.47	2007 Jun	7200	100	HB
R9		12.26	1.60	2007 Jun	900	115	RGB
R21		12.53	1.41	2007 Jun	1800	147	RGB
R90	IV-74	13.49	1.10	2000 Jun	1800	78	RGB
R100	I-25	13.58	1.07	2000 Jun	1800	105	RGB
R394	II-16	14.99	0.86	2000 Jun	7200	121	RGB
R431	IV-24	15.09	0.85	2000 Jun	5400	96	RGB
I-65		15.19	0.82	2000 Jun	7200	116	RGB

Table 2
Atomic Parameters and Equivalent Widths

Wavelength	Element	$\log gf$	EP	Ref.	A9	A11	A21	A25	
6300.30		8.0	-9.78	0.00	1	51.8	...
6363.78		8.0	-10.30	0.02	1	18.8	20.6	18.9	...
7771.94		8.0	0.37	9.15	1	...	14.2	19.5	17.9
7774.17		8.0	0.22	9.15	1	8.5	12.5	14.9	18.0
7775.39		8.0	0.00	9.15	1	...	6.0	8.9	11.6
5682.65		11.0	-0.70	2.10	2	78.40	68.40	33.60	32.00

References. — (1) Ramírez & Cohen 2003; (2) Ivans et al. 2006; (3) Ralchenko et al. 2008; (4) Aldenius et al. 2007; (5) Sneden et al. 2003; (6) Sobek et al. 2007; (7) Nilsson et al. 2006; (8) Fuhr & Wiese 2006; (9) Kurucz & Bell 1995; (10) Ljung et al. 2006; (11) Yong et al. 2008a

Note. — Table 2 is published in its entirety in the electronic edition. A portion is shown here for guidance regarding its form and content.

Table 3
Stellar Parameters and Radial Velocities

Name	T_{eff} (K)	$\log g$	v_t (km s ⁻¹)	[A/H]	Radial Velocity (km s ⁻¹)
A9	4236	0.61	2.28	-1.50	50.5
A11	4209	0.69	2.23	-1.50	60.0
A21	4381	1.05	1.82	-1.50	47.4
A25	4584	1.30	1.88	-1.50	52.5
A43	4630	1.44	1.85	-1.50	53.3
A65	4893	1.71	1.95	-1.50	54.9
A93	4961	1.84	1.87	-1.50	48.7
HB13	4740	1.82	1.35	-1.50	48.9
HB434	5400	2.36	2.06	-1.50	58.8
HB8	6100	2.63	3.38	-1.60	51.5
R9	4000	0.50	1.86	-1.35	54.7
R21	4100	0.66	1.81	-1.35	52.2
R90	4475	1.30	1.55	-1.40	57.2
R100	4525	1.46	1.55	-1.40	58.1
R394	4818	2.15	1.27	-1.40	51.7
R431	4845	2.20	1.24	-1.35	47.9
I-65	4860	2.25	1.20	-1.30	58.5

Table 4
Abundance Ratios [Fe/H] Through [O/Fe]

Star ID	[Fe/H]	<i>N</i>	[FeII/H]	<i>N</i>	log ϵ (Li)	<i>N</i>	$^{12}\text{C}/^{13}\text{C}$	<i>N</i>	[C/Fe]	<i>N</i>	[N/Fe]	<i>N</i>	[O/Fe]	<i>N</i>
A11	-1.56 ± 0.11	200	-1.47 ± 0.09	12	...	0	5.00 ± 2.00	2	0.14 ± 0.33	1	1.16 ± 0.42	1	0.49 ± 0.08	4
A21	-1.53 ± 0.11	208	-1.45 ± 0.08	19	...	0	4.50 ± 2.00	2	-0.17 ± 0.33	1	0.43 ± 0.36	1	0.47 ± 0.03	5
A25	-1.50 ± 0.11	203	-1.46 ± 0.12	17	...	0	5.00 ± 2.00	2	-0.27 ± 0.17	1	0.35 ± 0.23	1	0.31 ± 0.11	3
A43	-1.56 ± 0.11	228	-1.43 ± 0.11	26	...	0	6.00 ± 2.00	2	-0.04 ± 0.17	2	0.31 ± 0.23	1	0.56 ± 0.12	4
A65	-1.66 ± 0.11	144	-1.43 ± 0.11	19	...	0	...	0	-0.79 ± 0.17	2	1.36 ± 0.23	1	0.02 ± 0.19	2
A9	-1.49 ± 0.11	200	-1.49 ± 0.09	12	...	0	6.00 ± 2.00	1	-0.51 ± 0.30	2	0.99 ± 0.36	1	0.28 ± 0.11	2
A93	-1.59 ± 0.11	176	-1.48 ± 0.11	25	...	0	5.00 ± 2.00	1	-0.41 ± 0.17	2	0.89 ± 0.23	1	0.30 ± 0.10	4
HB13	-1.37 ± 0.11	222	-1.47 ± 0.11	24	...	0	...	0	-0.25 ± 0.22	1	0.57 ± 0.23	1	0.16 ± 0.11	3
HB434	-1.82 ± 0.10	150	-1.53 ± 0.08	23	...	0	...	0	-0.18 ± 0.31	1	< 0.92	1	0.72 ± 0.16	3
HB8	-1.77 ± 0.10	83	-1.60 ± 0.08	13	...	0	...	0	< 0.50	1	< 1.70	1	0.58 ± 0.12	3
R21	-1.30 ± 0.11	215	-1.32 ± 0.09	14	...	0	7.00 ± 2.00	1	-0.17 ± 0.33	1	-0.05 ± 0.36	1	0.29 ± 0.06	5
R9	-1.38 ± 0.11	192	-1.34 ± 0.09	11	...	0	6.00 ± 2.00	1	-0.34 ± 0.33	1	0.33 ± 0.42	1	-0.05 ± 0.15	1
R100	-1.40 ± 0.11	170	-1.36 ± 0.12	8	...	0	...	0	...	0	...	0	0.25 ± 0.16	1
R394	-1.51 ± 0.11	147	-1.35 ± 0.13	8	0.76 ± 0.21	1	...	0	...	0	...	0	0.14 ± 0.16	1
R431	-1.46 ± 0.11	144	-1.30 ± 0.12	7	0.96 ± 0.21	1	...	0	...	0	...	0	0.10 ± 0.16	1
R90	-1.38 ± 0.11	164	-1.45 ± 0.09	7	...	0	...	0	...	0	...	0	...	0
I-65	-1.40 ± 0.11	136	-1.22 ± 0.12	8	0.73 ± 0.21	1	...	0	...	0	...	0	...	0

Table 5
Abundance Ratios [Na/Fe] Through [Ti I/Fe]

Star Id	[Na/Fe]	<i>N</i>	[Mg/Fe]	<i>N</i>	[Al/Fe]	<i>N</i>	[Si/Fe]	<i>N</i>	[Ca/Fe]	<i>N</i>	[ScII/Fe]	<i>N</i>	[TiI/Fe]	<i>N</i>
A11	0.26 ± 0.06	5	0.42 ± 0.05	5	0.10 ± 0.12	2	0.48 ± 0.11	13	0.15 ± 0.05	13	0.04 ± 0.07	6	0.09 ± 0.07	46
A21	-0.08 ± 0.10	3	0.34 ± 0.06	5	-0.04 ± 0.12	2	0.40 ± 0.11	15	0.23 ± 0.05	14	0.08 ± 0.07	7	0.08 ± 0.07	48
A25	-0.01 ± 0.06	5	0.31 ± 0.05	6	0.06 ± 0.13	2	0.39 ± 0.08	15	0.23 ± 0.05	17	0.13 ± 0.06	9	0.17 ± 0.06	38
A43	-0.04 ± 0.09	4	0.32 ± 0.05	6	-0.12 ± 0.17	1	0.43 ± 0.09	16	0.25 ± 0.04	16	0.08 ± 0.06	10	0.17 ± 0.06	43
A65	0.49 ± 0.06	5	0.21 ± 0.07	5	0.70 ± 0.13	2	0.51 ± 0.09	13	0.33 ± 0.04	16	0.10 ± 0.05	9	0.13 ± 0.07	19
A9	0.29 ± 0.10	3	0.30 ± 0.09	6	0.30 ± 0.12	2	0.39 ± 0.12	14	0.18 ± 0.06	10	0.13 ± 0.08	7	0.17 ± 0.07	41
A93	0.35 ± 0.09	4	0.32 ± 0.05	7	0.18 ± 0.17	1	0.44 ± 0.09	14	0.26 ± 0.04	18	0.15 ± 0.05	10	0.18 ± 0.06	29
HB13	0.11 ± 0.07	6	0.25 ± 0.06	6	0.18 ± 0.13	2	0.30 ± 0.08	16	0.31 ± 0.04	19	0.28 ± 0.05	10	0.21 ± 0.06	50
HB434	0.22 ± 0.12	4	0.35 ± 0.05	7	0.10 ± 0.16	2	0.61 ± 0.11	3	0.36 ± 0.05	18	0.07 ± 0.07	9	0.25 ± 0.03	20
HB8	0.47 ± 0.11	2	0.44 ± 0.07	6	0.29 ± 0.16	1	0.32 ± 0.12	2	0.32 ± 0.04	12	0.23 ± 0.07	5	0.31 ± 0.09	3
R21	0.00 ± 0.06	5	0.32 ± 0.06	5	-0.11 ± 0.12	2	0.29 ± 0.11	15	0.25 ± 0.05	14	0.21 ± 0.06	6	0.26 ± 0.07	48
R9	0.50 ± 0.10	3	0.32 ± 0.05	5	0.57 ± 0.12	2	0.42 ± 0.12	14	0.24 ± 0.06	13	0.16 ± 0.06	5	0.19 ± 0.07	42
R100	0.25 ± 0.07	5	0.37 ± 0.16	1	0.17 ± 0.13	2	0.38 ± 0.09	15	0.35 ± 0.04	17	0.23 ± 0.05	7	0.23 ± 0.07	25
R394	-0.17 ± 0.10	3	0.35 ± 0.16	1	...	0	0.34 ± 0.09	18	0.35 ± 0.04	18	0.12 ± 0.05	7	0.24 ± 0.07	12
R431	-0.04 ± 0.09	4	0.54 ± 0.16	1	-0.07 ± 0.17	1	0.39 ± 0.09	16	0.37 ± 0.04	18	0.10 ± 0.05	7	0.23 ± 0.07	15
R90	0.37 ± 0.12	3	0.34 ± 0.16	1	0.54 ± 0.12	2	0.39 ± 0.11	17	0.35 ± 0.05	17	0.32 ± 0.06	7	0.18 ± 0.07	24
I-65	0.23 ± 0.10	4	0.32 ± 0.16	1	0.39 ± 0.17	1	0.41 ± 0.09	14	0.36 ± 0.04	18	0.15 ± 0.05	8	0.22 ± 0.06	13

Table 6
Abundance Ratios [TiII/Fe] Through [Co/Fe]

Star Id	[TiII/Fe]	<i>N</i>	[VI/Fe]	<i>N</i>	[VII/Fe]	<i>N</i>	[CrI/Fe]	<i>N</i>	[CrII/Fe]	<i>N</i>	[Mn/Fe]	<i>N</i>	[Co/Fe]	<i>N</i>
A11	0.18 ± 0.07	6	-0.22 ± 0.11	12	...	0	-0.14 ± 0.06	24	0.03 ± 0.11	2	-0.36 ± 0.07	8	0.00 ± 0.07	7
A21	0.26 ± 0.08	12	-0.23 ± 0.11	12	...	0	-0.10 ± 0.05	17	0.05 ± 0.10	3	-0.38 ± 0.07	8	-0.11 ± 0.09	4
A25	0.26 ± 0.06	14	-0.17 ± 0.09	9	...	0	-0.13 ± 0.05	18	0.01 ± 0.07	5	-0.34 ± 0.06	7	0.12 ± 0.14	3
A43	0.30 ± 0.06	21	-0.23 ± 0.09	15	...	0	-0.12 ± 0.06	20	-0.01 ± 0.05	8	-0.41 ± 0.05	9	-0.02 ± 0.11	5
A65	0.33 ± 0.07	18	-0.29 ± 0.12	3	...	0	-0.25 ± 0.03	12	0.01 ± 0.08	4	-0.43 ± 0.06	5	-0.02 ± 0.16	1
A9	0.24 ± 0.09	7	-0.23 ± 0.14	10	...	0	-0.11 ± 0.05	18	0.02 ± 0.16	1	-0.33 ± 0.08	8	0.07 ± 0.08	6
A93	0.35 ± 0.06	25	-0.26 ± 0.08	7	...	0	-0.17 ± 0.05	19	0.02 ± 0.05	9	-0.41 ± 0.06	7	-0.09 ± 0.16	1
HB13	0.39 ± 0.06	20	-0.12 ± 0.09	10	...	0	0.02 ± 0.04	26	0.14 ± 0.06	6	-0.34 ± 0.05	8	-0.17 ± 0.16	2
HB434	0.20 ± 0.05	32	-0.17 ± 0.11	2	-0.05 ± 0.17	1	-0.17 ± 0.05	15	-0.01 ± 0.05	8	-0.30 ± 0.06	8	-0.08 ± 0.11	2
HB8	0.39 ± 0.05	24	...	0	0.10 ± 0.17	1	-0.04 ± 0.07	7	0.05 ± 0.08	6	-0.45 ± 0.11	2	0.03 ± 0.16	1
R21	0.40 ± 0.08	8	-0.10 ± 0.11	11	...	0	0.00 ± 0.05	33	0.17 ± 0.16	1	-0.35 ± 0.09	4	0.03 ± 0.08	6
R9	0.29 ± 0.10	6	-0.11 ± 0.12	10	...	0	0.00 ± 0.05	23	0.11 ± 0.11	2	-0.51 ± 0.11	2	0.05 ± 0.08	6
R100	0.32 ± 0.09	4	0.02 ± 0.09	8	...	0	0.00 ± 0.06	10	0.03 ± 0.15	1	-0.38 ± 0.04	5	0.01 ± 0.11	2
R394	0.21 ± 0.10	3	-0.11 ± 0.08	8	...	0	-0.05 ± 0.06	7	-0.06 ± 0.15	1	-0.43 ± 0.08	4	-0.11 ± 0.16	1
R431	0.27 ± 0.10	3	-0.11 ± 0.11	4	...	0	-0.02 ± 0.05	8	-0.14 ± 0.15	1	-0.41 ± 0.08	4	0.15 ± 0.11	2
R90	0.29 ± 0.10	3	-0.01 ± 0.11	11	...	0	0.01 ± 0.06	9	0.08 ± 0.16	1	-0.37 ± 0.09	4	0.01 ± 0.08	5
I-65	0.32 ± 0.10	3	-0.10 ± 0.09	6	...	0	0.03 ± 0.07	7	-0.08 ± 0.15	1	-0.49 ± 0.04	5	0.17 ± 0.16	1

Table 7
Abundance Ratios [Ni/Fe] Through [ZrII/Fe]

Star Id	[Ni/Fe]	<i>N</i>	[Zn/Fe]	<i>N</i>	[Cu/Fe]	<i>N</i>	[SrI/Fe]	<i>N</i>	[YII/Fe]	<i>N</i>	[ZrI/Fe]	<i>N</i>	[ZrII/Fe]	<i>N</i>
A11	-0.06 ± 0.03	40	0.36 ± 0.27	2	-0.84 ± 0.11	2	...	0	-0.22 ± 0.07	5	0.04 ± 0.16	4	0.31 ± 0.18	2
A21	-0.08 ± 0.03	36	0.16 ± 0.19	2	-0.87 ± 0.11	2	-0.37 ± 0.17	1	-0.22 ± 0.06	8	-0.04 ± 0.16	3	0.38 ± 0.11	3
A25	-0.07 ± 0.05	32	0.05 ± 0.15	2	-0.87 ± 0.13	2	-0.34 ± 0.17	1	-0.27 ± 0.09	4	...	0	0.23 ± 0.11	2
A43	-0.08 ± 0.05	35	0.17 ± 0.15	2	-0.89 ± 0.13	2	-0.41 ± 0.17	1	-0.22 ± 0.05	7	...	0	0.38 ± 0.10	4
A65	-0.16 ± 0.07	12	0.25 ± 0.15	2	-0.94 ± 0.17	1	...	0	-0.31 ± 0.06	6	...	0	...	0
A9	-0.07 ± 0.03	37	0.07 ± 0.22	1	-0.87 ± 0.11	2	...	0	-0.33 ± 0.10	4	0.11 ± 0.16	4	0.48 ± 0.16	1
A93	-0.07 ± 0.05	21	0.11 ± 0.15	2	-0.92 ± 0.13	2	-0.47 ± 0.17	1	-0.26 ± 0.05	5	...	0	0.21 ± 0.05	5
HB13	-0.10 ± 0.05	28	0.15 ± 0.14	3	-0.83 ± 0.13	2	-0.41 ± 0.17	1	-0.09 ± 0.05	6	...	0	0.27 ± 0.11	2
HB434	-0.08 ± 0.08	4	0.18 ± 0.12	2	-0.88 ± 0.16	1	...	0	-0.29 ± 0.07	5	...	0	0.08 ± 0.10	4
HB8	-0.22 ± 0.09	3	...	0	< -0.33	1	...	0	0.05 ± 0.17	1	...	0	...	0
R21	-0.09 ± 0.03	44	0.06 ± 0.19	2	-0.93 ± 0.15	1	...	0	-0.09 ± 0.13	4	0.09 ± 0.16	4	...	0
R9	-0.06 ± 0.03	39	...	0	-0.92 ± 0.15	1	...	0	-0.11 ± 0.12	3	0.10 ± 0.16	3	...	0
R100	-0.03 ± 0.05	27	...	0	-0.94 ± 0.17	1	...	0	-0.21 ± 0.16	1	0.31 ± 0.16	2	...	0
R394	-0.05 ± 0.05	25	...	0	-1.04 ± 0.17	1	...	0	-0.18 ± 0.16	1	...	0	...	0
R431	-0.04 ± 0.05	23	...	0	-0.94 ± 0.17	1	...	0	...	0	...	0	...	0
R90	-0.03 ± 0.04	25	...	0	-0.99 ± 0.15	1	...	0	...	0	0.07 ± 0.21	1	...	0
I-65	0.00 ± 0.05	21	...	0	-1.05 ± 0.17	1	...	0	...	0	...	0	...	0

Table 8
Abundance Ratios [Mo/Fe] Through [PrII/Fe]

Star ID	[Mo/Fe]	<i>N</i>	[BaII/Fe]	<i>N</i>	[LaII/Fe]	<i>N</i>	[CeII/Fe]	<i>N</i>	[PrII/Fe]	<i>N</i>
A11	-0.14 ± 0.17	1	-0.04 ± 0.17	3	-0.22 ± 0.12	4	-0.16 ± 0.10	5	...	0
A21	-0.14 ± 0.17	1	0.09 ± 0.18	3	-0.03 ± 0.12	3	-0.14 ± 0.12	4	-0.01 ± 0.16	1
A25	...	0	0.09 ± 0.11	3	0.04 ± 0.10	3	-0.03 ± 0.12	4	...	0
A43	...	0	0.00 ± 0.11	3	-0.07 ± 0.09	4	-0.22 ± 0.11	7	...	0
A65	...	0	0.06 ± 0.11	3	-0.12 ± 0.10	3	-0.18 ± 0.12	4	...	0
A9	-0.04 ± 0.17	1	0.03 ± 0.17	3	-0.05 ± 0.12	3	-0.11 ± 0.12	3	...	0
A93	...	0	0.03 ± 0.10	4	0.00 ± 0.09	4	-0.07 ± 0.10	6	...	0
HB13	-0.21 ± 0.17	1	0.27 ± 0.11	3	0.18 ± 0.09	4	0.04 ± 0.10	7	...	0
HB434	...	0	0.01 ± 0.14	3	-0.12 ± 0.13	2	-0.31 ± 0.13	2	...	0
HB8	...	0	-0.02 ± 0.12	3	0.02 ± 0.13	2	...	0	...	0
R21	-0.13 ± 0.17	1	0.13 ± 0.17	3	0.00 ± 0.12	3	0.07 ± 0.11	6	0.30 ± 0.16	1
R9	-0.15 ± 0.17	1	0.05 ± 0.17	3	-0.02 ± 0.12	3	0.01 ± 0.12	3	0.34 ± 0.16	1
R100	0.06 ± 0.17	1	0.17 ± 0.12	3	0.06 ± 0.12	2	...	0	...	0
R394	...	0	0.10 ± 0.11	3	-0.24 ± 0.16	1	...	0	...	0
R431	...	0	0.10 ± 0.11	3	0.05 ± 0.16	1	...	0	...	0
R90	-0.05 ± 0.17	1	0.31 ± 0.17	3	0.09 ± 0.17	1	...	0	...	0
I-65	...	0	0.21 ± 0.11	3	0.07 ± 0.16	1	...	0	...	0

Table 9
Abundance Ratios [NdII/Fe] Through [ThII/Fe]

Star ID	[NdII/Fe]	<i>N</i>	[SmII/Fe]	<i>N</i>	[EuII/Fe]	<i>N</i>	[DyII/Fe]	<i>N</i>	[ThII/Fe]	<i>N</i>
A11	-0.08 ± 0.10	10	0.14 ± 0.11	3	0.37 ± 0.17	1	...	0	0.22 ± 0.22	1
A21	0.10 ± 0.10	8	0.34 ± 0.10	4	0.50 ± 0.13	2	...	0	...	0
A25	0.10 ± 0.09	7	0.31 ± 0.12	4	0.47 ± 0.13	2	...	0	...	0
A43	-0.03 ± 0.10	15	0.12 ± 0.13	3	0.38 ± 0.13	2	0.32 ± 0.17	1	...	0
A65	-0.05 ± 0.11	6	0.09 ± 0.15	2	0.33 ± 0.12	3	0.30 ± 0.17	1	...	0
A9	0.03 ± 0.11	8	0.21 ± 0.13	2	0.47 ± 0.13	2	...	0	0.29 ± 0.22	1
A93	0.08 ± 0.10	9	0.17 ± 0.15	2	0.38 ± 0.13	2	0.43 ± 0.17	1	...	0
HB13	0.18 ± 0.10	13	0.31 ± 0.12	5	0.52 ± 0.13	2	0.60 ± 0.17	1	...	0
HB434	0.01 ± 0.13	2	...	0	0.31 ± 0.17	1	0.15 ± 0.17	1	...	0
HB8	...	0	...	0	0.55 ± 0.17	1	...	0	...	0
R21	0.12 ± 0.11	8	0.33 ± 0.11	3	0.52 ± 0.17	1	...	0	0.31 ± 0.22	1
R9	0.10 ± 0.12	3	0.29 ± 0.17	1	0.47 ± 0.17	1	...	0	0.34 ± 0.22	1
R100	0.12 ± 0.14	2	...	0	0.51 ± 0.17	1	...	0	...	0
R394	-0.03 ± 0.17	1	...	0	0.27 ± 0.17	1	...	0	...	0
R431	-0.02 ± 0.17	1	...	0	0.45 ± 0.17	1	...	0	...	0
R90	0.18 ± 0.17	1	...	0	0.55 ± 0.17	1	...	0	...	0
I-65	-0.08 ± 0.17	1	...	0	0.47 ± 0.17	1	...	0	...	0

Table 10
Average Abundance Values

Element	[X/Fe] total	σ total	N total	[X/Fe] AGB	σ AGB	N AGB	[X/Fe] RGB	σ RGB	N RGB	[X/Fe] HB	σ HB	N HB
FeI	-1.51	0.14	17	-1.53	0.08	8	-1.40	0.07	7	-1.80	0.04	2
FeII	-1.42	0.09	17	-1.46	0.02	8	-1.33	0.07	7	-1.57	0.05	2
C	-0.27	0.25	11	-0.29	0.29	8	-0.25	0.12	2	-0.18	...	1
N	0.63	0.45	10	0.76	0.40	8	0.14	0.27	2
O	0.31	0.22	15	0.32	0.18	8	0.15	0.13	5	0.65	0.10	2
Na	0.19	0.21	17	0.17	0.21	8	0.16	0.24	7	0.34	0.18	2
Mg	0.34	0.07	17	0.31	0.06	8	0.37	0.08	7	0.39	0.06	2
Al	0.20	0.25	16	0.17	0.25	8	0.25	0.30	6	0.19	0.13	2
Si	0.41	0.08	17	0.42	0.06	8	0.37	0.05	7	0.47	0.21	2
Ca	0.29	0.07	17	0.24	0.06	8	0.32	0.05	7	0.34	0.03	2
ScII	0.15	0.08	17	0.12	0.07	8	0.18	0.08	7	0.15	0.11	2
TiI	0.19	0.06	17	0.15	0.05	8	0.22	0.03	7	0.28	0.04	2
TiII	0.29	0.07	17	0.29	0.07	8	0.30	0.06	7	0.29	0.13	2
VI	-0.15	0.09	16	-0.22	0.05	8	-0.07	0.06	7	-0.17	...	1
VII	0.03	0.11	2	0.03	0.11	2
CrI	-0.07	0.08	17	-0.12	0.08	8	-0.00	0.03	7	-0.11	0.09	2
CrII	0.02	0.08	17	0.03	0.05	8	0.02	0.11	7	0.02	0.04	2
Mn	-0.39	0.06	17	-0.38	0.04	8	-0.42	0.06	7	-0.38	0.11	2
Co	0.00	0.09	17	-0.03	0.09	8	0.04	0.09	7	-0.02	0.08	2
Ni	-0.08	0.05	17	-0.09	0.03	8	-0.04	0.03	7	-0.15	0.10	2
Zn	0.16	0.11	10	0.17	0.12	8	0.06	...	1	0.18	...	1
Cu	-0.92	0.06	16	-0.88	0.04	8	-0.97	0.05	7	-0.88	...	1
Sr	-0.40	0.05	5	-0.40	0.05	5
YII	-0.20	0.10	14	-0.24	0.07	8	-0.15	0.06	4	-0.12	0.24	2
ZrI	0.10	0.11	7	0.04	0.08	3	0.14	0.11	4
ZrII	0.29	0.12	8	0.32	0.10	7	0.08	...	1
Mo	-0.10	0.08	8	-0.13	0.07	4	-0.07	0.10	4
BaII	0.09	0.10	17	0.07	0.09	8	0.15	0.09	7	-0.00	0.02	2
LaII	-0.02	0.11	17	-0.03	0.12	8	0.00	0.11	7	-0.05	0.10	2
CeII	-0.10	0.12	11	-0.11	0.09	8	0.04	0.04	2	-0.31	...	1
PrII	0.21	0.19	3	-0.01	...	1	0.32	0.03	2
NdII	0.05	0.09	16	0.04	0.09	8	0.06	0.10	7	0.01	...	1
SmII	0.23	0.10	10	0.21	0.10	8	0.31	0.03	2
EuII	0.44	0.09	17	0.43	0.07	8	0.46	0.09	7	0.43	0.17	2
DyII	0.36	0.17	5	0.41	0.14	4	0.15	...	1
ThII	0.29	0.05	4	0.25	0.05	2	0.32	0.02	2

Table 11
Comparisons to Previous Studies for A11 (IV-59)

Parameter/ Abundance	This Study	This Study (MARCS)	Ivans et al. (2001)	Ramírez & Cohen (2003)
T_{eff}	4209	4209	4229	4265
$\log g$	0.69	0.69	0.79	1.00
v_t	2.23	2.07	2.10	1.94
[Fe I/H]	-1.56	-1.60	-1.40	-1.40
[Fe II/H]	-1.47	-1.46	-1.25	-1.35
[O I/Fe]	0.49	0.53	0.37	0.36
[Na I/Fe]	0.26	0.23	0.13	0.09
[Mg I/Fe]	0.42	0.40	...	0.29
[Si I/Fe]	0.48	0.50	0.23	0.30
[Ca I/Fe]	0.15	0.08	0.21	0.03
[Sc II/Fe]	0.04	0.04	-0.19	0.31
[Ti I/Fe]	0.09	-0.01	0.08	0.01
[V I/Fe]	-0.23	-0.34	-0.21	-0.29
[Cr I/Fe]	-0.14	-0.17	...	-0.25
[Mn I/Fe]	-0.36	-0.41	-0.45*	-0.52
[Co I/Fe]	0.00	-0.01	...	-0.13
[Ni I/Fe]	-0.06	-0.05	-0.14	-0.03
[Cu I/Fe]	-0.84	-0.90	...	-0.58
[Zn I/Fe]	0.36	0.41	...	0.44
[Zr I/Fe]	0.04	-0.08	...	0.00
[Ba II/Fe]	-0.04	-0.03	0.10	0.19
[Eu II/Fe]	0.37	0.36	...	0.58

* From Sobek et al. (2006).

Table 12
[X/Eu]

Element	\langle [X/Eu] \rangle This Study	σ	N Stars	[X/Eu] [*] s.s. r -process	s.s. r -process [*] (%)	s.s. s -process [*] (%)
Sr	-0.80	0.14	5	-0.94	11.0	89.0
Y	-0.63	0.09	14	-0.54	28.1	71.9
Zr	-0.25	0.14	12	-0.52	19.1	80.9
Mo	-0.59	0.09	8	-0.48	32.3	67.7
Ba	-0.35	0.09	17	-0.82	14.7	85.3
La	-0.46	0.06	17	-0.60	24.6	75.4
Ce	-0.53	0.07	11	-0.72	18.6	81.4
Pr	-0.29	0.20	3	-0.28	50.8	49.2
Nd	-0.39	0.07	16	-0.36	42.1	57.9
Sm	-0.21	0.04	10	-0.16	66.9	33.1
Dy	-0.02	0.10	5	-0.04	87.9	12.1
Th	-0.17	0.04	4	0.02	100.0	...

^{*} From Simmerer et al. (2004).